Notes on n-point Witten diagrams in AdS$_2$

Gabriel Bliard[*]

Institut für Physik, Humboldt-Universität zu Berlin and IRIS Adlershof, Zum Großen Windkanal 2, 12489 Berlin, Germany

E-mail: gabriel.bliard@physik.hu-berlin.de

CrossMark

Abstract

Witten diagrams provide a perturbative framework for calculations in anti-de-Sitter space and play an essential role in a variety of holographic computations. In the case of this study in AdS$_2$, the one-dimensional boundary allows for a simple setup, in which we obtain perturbative analytic results for correlators with the residue theorem. This elementary method is used to find all scalar n-point contact Witten diagrams for external operators of conformal dimensions $\Delta = 1$ and $\Delta = 2$, and to determine topological correlators of Yang–Mills in AdS$_2$. Another established method is applied to explicitly compute exchange diagrams and give an example of a Polyakov block in $d = 1$. We also check perturbatively a recently proposed multipoint Ward identity with the strong coupling expansion of the six-point function of operators inserted on the 1/2 BPS Wilson line in $\mathcal{N} = 4$ SYM.

Keywords: holography, AdS$_2$, n-point correlators, CFT$_1$, Witten diagram, AdS integrals

(Some figures may appear in colour only in the online journal)

1. Discussion

The two-dimensional anti-de-Sitter space AdS$_2$ provides a wonderful playground both to study quantum field theory in curved space and to further our understanding of correlation functions in AdS/CFT. As there are no propagating degrees of freedom for the graviton, the latter is not a usual gauge/gravity correspondence, but rather a rigid holography that has physical settings e.g. in the context of defects in higher-dimensional theories [1–6], effective and intrinsic theories in AdS$_2$ [7–18]. Perturbative computations in anti-de-Sitter space are done through Witten

---

[*]Author to whom any correspondence should be addressed.

diagrams, whose structure has extensively been studied [19–29]. Yet, the complexity relative to their flat space counterpart is still a roadblock to perturbative analysis and there is still a search for the full equivalent of Feynman rules [30]. As such, the most efficient methods to date for perturbative correlators are through the conformal bootstrap [31, 32]. However, explicit computations remain a reliable way to make progress in perturbation theory and can provide some insight into assumptions that may simplify the bootstrap process. First-order four-point correlators with quartic interactions in the strong coupling limit can be written in terms of D-functions [21] which are four-point Witten contact diagrams. At higher order, with loops and exchanges which correspond to additional integrated bulk points, some diagrams can be related to contact integrals through differential equations [22, 33]. As such, the n-point D-functions are used beyond the first order and can be seen as a starting point to build 'master integrals' for Witten diagrams. AdS$_2$ is a perfect place to look at these integrals as it provides a simple framework with relevance in its own right (e.g. in defect theories) and corresponds to a diagonal limit ($z = \bar{z}$ for four points) of its higher-dimensional counterparts.

Boundary correlators in AdS$_2$ enjoy a one-dimensional conformal symmetry. In higher dimensions, along with additional symmetries, this simplifies perturbative computations. However, the structure of AdS$_2$ provides a framework in which another elementary method can be used to compute perturbative quantities; the residue theorem. Using contour integration for one of the AdS$_2$ integrals, the contact diagram in $\lambda_n \phi_\Delta^n$ theory for n scalars of low conformal dimension is remarkably simple leading to the results (see section 3 below)

$$\tilde{I}_{\Delta=1,n}(x_i) = \frac{(C_{\Delta=1})^n \pi}{(2i)^{n-2}} \sum_{i \neq j} \frac{(x_i - x_j)^{n-4}}{\prod_{k \neq i \neq j}(x_i - x_k)(x_k - x_j)} \ln\left(\frac{x_i - x_j}{2i}\right), \tag{1.1}$$

$$\tilde{I}_{\Delta=2,n}(x_i) = \sum_{j \neq i} \frac{-\pi(C_{\Delta=2})^n}{2(2i)^{2n-4}(x_i - x_j)^2} \partial_{x_j}\left(\frac{(x_j - x_i)^{2n-5}}{\prod_{k \neq j, k \neq i}(x_k - x_j)^2(x_k - x_i)^2} \ln\frac{x_j - x_i}{2i}\right) \tag{1.2}$$

$$+ \sum_{j \neq i} \partial_{x_i} \frac{-\pi(C_{\Delta=2})^n}{(2i)^{2n-2}(x_i - x_j)^2} \partial_{x_j}\left(\frac{(x_j - x_i)^{2n-4}}{\prod_{k \neq j, k \neq i}(x_k - x_j)^2(x_i - x_k)^2} \ln\frac{x_j - x_i}{2i}\right).$$

Above, $\tilde{I}_{\Delta,n}(x_i)$ is the integral corresponding to the Witten contact diagram of n fields ϕ_Δ of conformal dimension Δ inserted at positions x_i, and C_Δ is the conformal propagator normalisation defined in (2.22). These expressions are in terms of the operators' positions and combine naturally into the cross-ratios obtained with the usual conformal transformations (see discussion in section 2.1 around equation (2.5) and appendix A.2).

This method proves to be even more powerful in some settings where the residue theorem can be used for both of the bulk coordinates. This is the case for the topological three-point correlator of the boundary fields a of the gauge field of pure Yang–Mills in AdS$_2$ presented in [34], providing an alternative derivation in section 4 of

$$\langle a^a(x_1)a^b(x_2)a^c(x_3)\rangle = -\frac{1}{4\pi g_{YM}^2} f^{abc} \operatorname{sgn}(x_{12}x_{23}x_{31}), \tag{1.3}$$

where f^{abc} are the structure constants of the gauge group of the Yang–Mills theory. The low dimensionality has other advantages, such as having fewer cross-ratios. For four-point functions, for example, the single cross-ratio simplifies the differential equation used to compute exchange diagrams in section 5. We thus compute explicitly a Polyakov block corresponding to the sum of four-point exchange Witten diagrams with dimensions $\Delta = 1$, which agrees with

independently found results[1]

$$P_{1,1}^{(0)}(z) = \text{Li}_2\left(\frac{z}{z-1}\right)\log\left(\frac{z^2}{(z-1)^2}\right) - 6\text{Li}_3\left(\frac{z}{z-1}\right) - \frac{1}{6}\pi^2 \log\left(\frac{z^2}{(z-1)^2}\right) + 6\zeta(3)$$

$$+ \frac{\text{Li}_2(1-z)\log\left((z-1)^2\right) - 6\text{Li}_3(1-z) - \frac{1}{6}\pi^2 \log\left((z-1)^2\right) + 6\zeta(3)}{z^2}$$

$$+ \frac{\text{Li}_2(z)\log\left(z^2\right) - 6\text{Li}_3(z) - \frac{1}{6}\pi^2 \log\left(z^2\right) + 6\zeta(3)}{(z-1)^2}. \tag{1.4}$$

Natural extensions to this work include deriving position space results of contact diagrams in the case of higher external dimensions and Polyakov blocks for higher exchanged dimensions. A possible path for this is by extending the one-dimensional Mellin analysis developed in [35] to higher n-point functions using results from this study. In the former, Mellin amplitudes for higher Δ were obtained, so that, in combination with these notes, results for all (n, Δ) may be achievable. The knowledge of the structure of contact diagrams also sheds light on the computation of higher-point exchange diagrams through the method presented in section 5. A combination of these two techniques for contact and exchange diagrams could also, along with multipoint Ward identities and bootstrap methods, provide a path to the computation of the strong coupling, second-order, six-point correlator of the 1/2-BPS defect in $\mathcal{N} = 4$ SYM. In this spirit, an appendix is included providing a perturbative check of the consistency of the multipoint Ward identities conjectured in [36] for the first two strong coupling perturbative orders of the six-point correlator of insertions on the 1/2 BPS line in $\mathcal{N} = 4$ SYM. The higher-order quantities are beyond the scope of this paper and are left for further investigation.

The paper will proceed as follows; after an introduction to the basics, techniques, and notations of CFT_1 and AdS_2 in section 2, contour integration will be used in section 3 to derive the AdS_2 massless n-point contact diagrams which are consistent with the numerical integration and the current literature. This method will also be used in section 4 to derive the topological three-point correlator of the boundary field of pure Yang–Mills in AdS_2. Finally, known methods will be applied in section 5 to find the explicit expression of a one-dimensional Polyakov block, which has the correct symmetries, Regge behaviour, and double-discontinuity. Several technical appendices complete the manuscript.

2. Review of AdS$_2$/CFT$_1$ correlators

Interacting fields propagating in AdS_2 define a non-local one-dimensional conformal field at the boundary. We go through some basics of one-dimensional conformal theories, dynamics in two-dimensional anti-de-Sitter space, and set up the notation of this paper. We also review the concepts of Polyakov blocks and the methods used in [26, 33] to relate AdS exchange diagrams to contact diagrams in the context of CFT_1.

2.1. CFT$_1$ basics, techniques, and notation

A one-dimensional conformal field theory can be defined by a set of data consisting of the spectrum $\{\Delta\}$ which defines which operators are present in the theory, and the coefficients $\{c_{\Delta_1 \Delta_2 \Delta_3}\}$ which define the interactions of these operators. Combined with the operator product expansion (OPE), these can be used to reconstruct any correlator of local operators in the

---

[1] We thank Pietro Ferrero for sharing some of the unpublished results related to [10].

theory. The conformal group in $d = 1$ is generated by the translation P, dilation D, and special conformal transformation K which satisfy the conformal algebra and can be parametrised in one dimension by the differential operators

$$P = -\partial_x \qquad D = -x\partial_x - \Delta \qquad K = -x^2\partial_x - 2\Delta x, \tag{2.1}$$

when acting on a field of conformal dimension Δ evaluated at position x. The consequence of these symmetries on correlators is that the coordinate dependence of the first three n-point correlators is fixed

$$\langle \phi_\Delta(x) \rangle = \delta_{\Delta,0} \tag{2.2}$$

$$\langle \phi_{\Delta_1}(x_1)\phi_{\Delta_2}(x_2) \rangle = \frac{\delta_{\Delta_1,\Delta_2}}{x_{12}^{2\Delta}} \tag{2.3}$$

$$\langle \phi_{\Delta_1}(x_1)\phi_{\Delta_2}(x_2)\phi_{\Delta_3}(x_3) \rangle = \frac{c_{\Delta_1\Delta_2\Delta_3}}{(x_{12})^{\Delta_{123}}(x_{13})^{\Delta_{132}}(x_{23})^{\Delta_{231}}} \qquad \Delta_{ijk} = \Delta_i + \Delta_j - \Delta_k. \tag{2.4}$$

For n-point correlators, conformal transformations can be used to reduce the number of independent variables to $n - 3$ conformally invariant cross-ratios

$$u_i = \frac{x_{1i}x_{n-1,n}}{x_{in}x_{1,n-1}} \qquad 0 < u_i < 1, \tag{2.5}$$

where $x_{ij} = x_j - x_i$ are real numbers in $d = 1$. For equal conformal dimensions the correlator is[2]

$$\langle \phi_\Delta(x_1)..\phi_\Delta(x_i)\ldots\phi_\Delta(x_n) \rangle = A(x_1,\ldots,x_n)\langle \phi_\Delta(0)..\phi_\Delta(u_i)\ldots\phi_\Delta(1)\tilde{\phi}_\Delta(\infty) \rangle, \tag{2.7}$$

where

$$A(x_1,\ldots x_n) = \left(\left(\frac{x_{1n}x_{n-1,n}}{x_{1,n-1}} \right)^{n-2} \prod_{j=1}^{n-1} x_{jn}^{-2} \right)^{\Delta}. \tag{2.8}$$

One might wonder why higher-point correlators are of any interest since the theory can be determined by the set $\{\Delta, c_{\Delta_1\Delta_2\Delta_3}\}$. In practice, however, determining such a set is far from trivial, and working out perturbative higher-point correlators gives access to this information through the dynamics of the theory. For example, the four-point correlator has the following OPE

$$\langle \phi_\Delta(x_1)\phi_\Delta(x_2)\phi_\Delta(x_3)\phi_\Delta(x_4) \rangle = \frac{1}{(x_{13}x_{24})^{2\Delta}}f(z) \tag{2.9}$$

$$f(z) = \sum_h c_{\Delta\Delta h}^2 z^{h-2\Delta}\,_2F_1(h,h,2h;z), \tag{2.10}$$

---

[2] Note that the limit

$$\lim_{\epsilon \to 0}\langle \phi_\Delta(x_1)..\phi_\Delta(x_i)\ldots\epsilon^{-2\Delta}\phi_\Delta(\epsilon^{-1}) \rangle = \langle \phi_\Delta(x_1)..\phi_\Delta(x_i)\ldots\tilde{\phi}_\Delta(\infty) \rangle \tag{2.6}$$

is well defined.

where $z = \frac{x_{12}x_{34}}{x_{13}x_{24}}$ is the usual cross-ratio—u_2 in (2.5)—for the four-point function in 1D. When computing the analytic expression of this four-point correlator at different orders in perturbation theory, for example using Witten diagrams in a holographic setup [1, 4], these can be equated to the expansion of (2.9) to find the perturbative CFT data $\{\Delta, c_{\Delta_1 \Delta_2 \Delta_3}\}$.

The symmetries of the conformal blocks (similarity under $z \to \frac{z}{z-1}$), those of the correlator (crossing symmetry under $z \to 1 - z$), and those of the theory (e.g. Ward identities in [2]) can be used to highly constrain the four-point correlators. Complemented by a transcendentality ansatz for the correlators [37], this provides a powerful way to compute perturbative correlators, as was done in [2, 4, 6, 10, 38].

The bosonic four-point correlator defined in (2.9) has symmetries under the permutations of the external operators. Given the ordering of the operators, the variable z is naturally defined on the range $0 < z < 1$. Following the analysis of [39], the bosonic symmetry can be used to define the function in (2.11) on the entire real axis.

$$
f(z) = \begin{cases} f^{(-)}(z) = (1-z)^{2\Delta} f^{(0)}\left(\dfrac{z}{z-1}\right) & z < 0 \\[2mm] f^{(0)}(z) & 0 < z < 1 \\[2mm] f^{(+)}(z) = z^{2\Delta} f^{(0)}\left(\dfrac{1}{z}\right) & z > 1 \end{cases} \tag{2.11}
$$

The resulting function has an explicit symmetry under crossing

$$
z \to 1 - z \quad 0 < z < 1, \tag{2.12}
$$

and braiding

$$
z \to \frac{z}{z-1}. \tag{2.13}
$$

These two symmetries generate all the crossing symmetries from bosonic permutations. In addition, these functions defined on a segment of the real line can be analytically continued outside their region of analyticity. For some functions (for example, those resulting from contact Witten diagrams), the analytic continuation of the function $f^{(0,\pm)}(z)$ outside its segment of definition matches the function $f(z)$. In this case, we speak of *braiding symmetry*. This is linked to the vanishing of the double-discontinuity, defined in [39] as

$$
\mathrm{dDisc}^+[\mathcal{G}(z)] = \mathcal{G}^{(0)}(z) - \frac{\mathcal{G}^{(+)}(z + i\epsilon) + \mathcal{G}^{(+)}(z - i\epsilon)}{2} \quad 0 < z < 1. \tag{2.14}
$$

Unitarity arguments link this double-discontinuity to the full correlator thanks to the inversion formula [39] and provide a powerful tool constraining the correlators and correspondingly the OPE data.

The OPE expansion is the projection of the correlator on the basis of the conformal blocks. There is, however, another basis that is of some interest in this context; Polyakov blocks. These are defined to be crossing-symmetric, Regge-bounded[3], and to have the same expansion as the

---

[3] The Regge limit of a correlator in $d = 1$ is controlled by its behaviour at large $|z|$. A Regge bounded correlator $g(z)$ satisfies $\lim_{\zeta \to \infty} g(\frac{1}{2} + i\zeta) < C$ where C is a constant. Note that the identity contribution has a constant contribution in this limit.

conformal blocks (see for example section 6 of [39])

$$\sum_h c_h G_h(z) = \sum_h c_h P_h(z). \tag{2.15}$$

Their existence in $d = 1$ was motivated in [32, 40, 41] and proven in [42]. Additionally, they have the same double-discontinuity as the conformal blocks and have a double zero at the position of double trace operators

$$P_{2\Delta+2n} = 0 \tag{2.16}$$

$$\partial_n P_{2\Delta+n} = \delta_{n,0}. \tag{2.17}$$

As a consequence, they can be expressed as the sum of Witten exchange diagrams (see the example of perturbative Polyakov blocks in appendix B.2). Through the computation of the exchange Witten diagrams in position space in one dimension, the explicit form of a Polyakov block is shown below in section 5.

2.2. Witten diagrammatics in AdS$_2$

We consider bulk theories in euclidean AdS$_2$, for which we use the Poincaré metric

$$ds^2_{\text{AdS}_2} = \frac{dx^2 + dz^2}{z^2}. \tag{2.18}$$

Scalar bosonic fields of mass m are dual to conformal scalars of dimension Δ

$$m^2 = \Delta(\Delta - 1), \tag{2.19}$$

inserted on the boundary ($z = 0$). These fields have a bulk-to-bulk propagator

$$G^\Delta_{BB}(a, b) = C_\Delta (2u)^{-1}{}_2F_1(\Delta, \Delta, 2\Delta, -2u^{-1}) \ u = \frac{(z_a - z_b)^2 + (x_a - x_b)^2}{2z_a z_b}, \tag{2.20}$$

which satisfies the AdS$_2$ equation of motion

$$(\nabla^2_{\text{AdS}} - \Delta(\Delta - 1))G^\Delta_{BB}(a, b) = z^2 \delta^{(2)}(a - b), \tag{2.21}$$

and whose normalisation [29, 43] is

$$C_\Delta = \frac{\Gamma(\Delta)}{2\sqrt{\pi}\Gamma\left(\Delta + \frac{1}{2}\right)}. \tag{2.22}$$

The bulk-to-boundary propagator corresponding to the $z \to 0$ limit of (2.20) is

$$K_\Delta(z, x; x_i) = C_\Delta \tilde{K}_\Delta(z, x; x_i) \tag{2.23}$$

$$= C_\Delta \left(\frac{z}{z^2 + (x - x_i)^2}\right)^\Delta. \tag{2.24}$$

Due to the isometries of AdS$_2$, the boundary correlators will be conformal. Given an action, for example the effective worldsheet theory on AdS$_2$ of [1], boundary correlators are computed via Witten diagrams (e.g. the contact diagram in figure 1).

Just as in Feynman diagrams, the external legs, propagators and vertices play the same role. The external legs are depicted as points at the boundary and the integral is evaluated over the
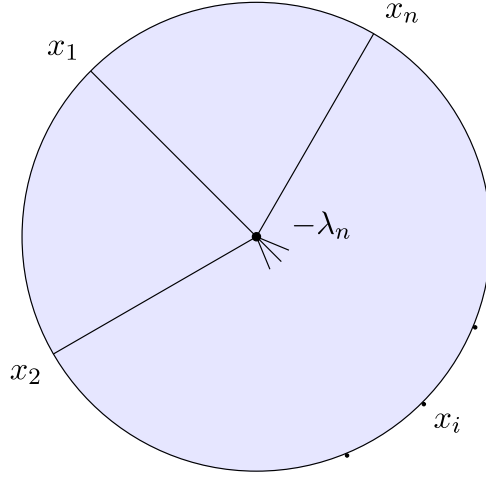
Figure 1. Witten n-point contact diagram with a $\lambda_n \phi^n$ interaction and n boundary insertions at positions $\{x_1, \ldots, x_n\}$.

position of the vertices in the bulk of AdS$_2$. For example, the contact diagram depicted in figure 1 corresponds to the integral

$$\lambda_n \tilde{I}_{\Delta,n}(x_1, \ldots, x_n) = \lambda_n \int \frac{\mathrm{d}z\,\mathrm{d}x}{z^2} \prod_{i=1}^{n} K_\Delta(z, x; x_i), \tag{2.25}$$

which will be solved in section 3 for all n and $\Delta = 1, 2$.

The first extension to this class of integrals is to consider multiple bulk integrations. This happens when there are loops and exchanges in the corresponding Witten diagram. For some exchange diagrams, the multiple integrals can be related to (2.25) through the action of a differential operator (for more details see appendix B.1). For example, the four-point single-exchange diagram can be found by solving the differential equation

$$(C_{(34)}^{(2)} - m_{\mathrm{E}}^2) J(x_1, x_2, x_3, x_4) = \int \frac{\mathrm{d}z_a\,\mathrm{d}x_a}{z_a^2} \Pi_{i=1}^4 K_{\Delta_\phi}(z_a, x_a; x_i) \tag{2.26}$$

$$= \tilde{I}_{\Delta_\phi, 4}(z), \tag{2.27}$$

where $C_{34}^{(2)}$ is the quadratic Casimir acting on the external legs 3 and 4, m_{E} is the mass of the exchanged operator, and the full integral is given by

$$J(x_1 \ldots x_4) = \int \frac{\mathrm{d}z_a\,\mathrm{d}x_a}{z_a^2} \int \frac{\mathrm{d}z_b\,\mathrm{d}x_b}{z_b^2} G_{BB}^{\Delta_{\mathrm{E}}}(a, b) \prod_{i=1}^{2} \left(K_{\Delta_\phi}(z_a, x_a; x_i) \right) \prod_{i=3}^{4} \left(K_{\Delta_\phi}(z_b, x_b; x_i) \right). \tag{2.28}$$

The simple structure of one-dimensional conformal correlators allows us to write the result explicitly in position space for the case $\Delta = \Delta_{\mathrm{E}} = 1$, see below in (5.15).

These quantities have been computed in Mellin space [10, 24, 28, 29, 44], where Witten diagrams have a natural language. In particular, contact diagrams with no derivatives are given by constant truncated Mellin amplitudes and exchange diagrams have poles in Mellin space[4].

However, there are several caveats to these results. Firstly, the Mellin and anti-Mellin transforms are not trivial computations, so knowledge of the Mellin amplitude does not imply that of the position space correlator and vice-versa. Additionally, the generality of such results prevents the use of the simplifications occurring in $d = 1$. Furthermore, when the number of external legs is large enough ($n > d + 2$), many spurious Mellin variables do not correspond to a cross-ratio in position space. This is already relevant for the four-point $d = 1$ correlator. In one dimension, several attempts were made to use the Mellin transform using the higher-dimensional formalism [10] or developing a one-dimensional formalism [35]. Using as a guide the principle that contact Witten diagrams correspond to constant Mellin amplitudes, the results in section 3 may provide a starting point in generalising the one-dimensional Mellin formalism developed in [35]. There, results for contact diagrams with general external dimensions Δ were derived so that, in combination with the insights of the present study, results for all (n, Δ) may be achievable.

3. n-point contact diagrams

We start by looking at n-point correlators of identical scalars with a simple contact interaction. These will serve not only as examples to demonstrate the simplifications occurring in this low-dimensional case, but also as building blocks for the massive contact diagrams, exchange diagrams, and other cases seen in the following sections. These correlators result from an interaction term $\lambda_n \phi^n$ in the bulk of AdS_2 and will be a function of $n - 3$ independent cross-ratios due to the symmetry structure of CFT_1, or equivalently, the isometry structure of AdS_2. These constitute the 'master integrals' in AdS_2 for contact diagrams used in [1, 4]. The contact diagram is illustrated in figure 1 and can be written as an integration over AdS_2 of the n bulk-to-boundary propagators, leading to the connected tree-level correlator

$$\langle\phi_{\Delta_1}(x_1)\dots\phi_{\Delta_n}(x_n)\rangle^{(1)}_{\text{conn}} = -\lambda_n\left(\Pi^n_{i=1}C_{\Delta_i}\right)I_{\Delta_1,\dots,\Delta_n}(x_1,\dots,x_n),\tag{3.1}$$

where we define the integral

$$I_{\Delta_1,\dots,\Delta_n}(x_1,\dots,x_n) = \int\frac{\mathrm{d}x\,\mathrm{d}z}{z^2}\Pi^n_{i=1}\left(\frac{z}{z^2+(x-x_i)^2}\right)^{\Delta_i}.\tag{3.2}$$

The simplifications of AdS_2 can be made explicit by evaluating the x-integral first with contour integration. This is especially effective for the massless case ($\Delta = 1$) where the integrand of (3.2) only has single poles and the general result—see (3.24) below—for a massless n-point function is derived,

$$\langle\phi_{\Delta=1}(x_1)\dots\phi(x_n)\rangle = \begin{cases} -\lambda_n\dfrac{\pi(C_{\Delta=1})^n}{(2i)^{n-2}}\displaystyle\sum_{i>j}\frac{(x_i-x_j)^{n-4}}{\Pi^n_{k\neq i\neq j}(x_i-x_k)(x_j-x_k)}\ \ln\left((x_i-x_j)^2\right) & n\text{ even} \\[20pt] -\lambda_n\dfrac{\pi^2(C_{\Delta=1})^n}{2(2i)^{n-3}}\displaystyle\sum^n_{i>j}\frac{(x_i-x_j)^{n-4}}{\Pi_{k\neq j\neq i}(x_k-x_j)(x_k-x_i)} & n\text{ odd.} \end{cases}\tag{3.3}$$

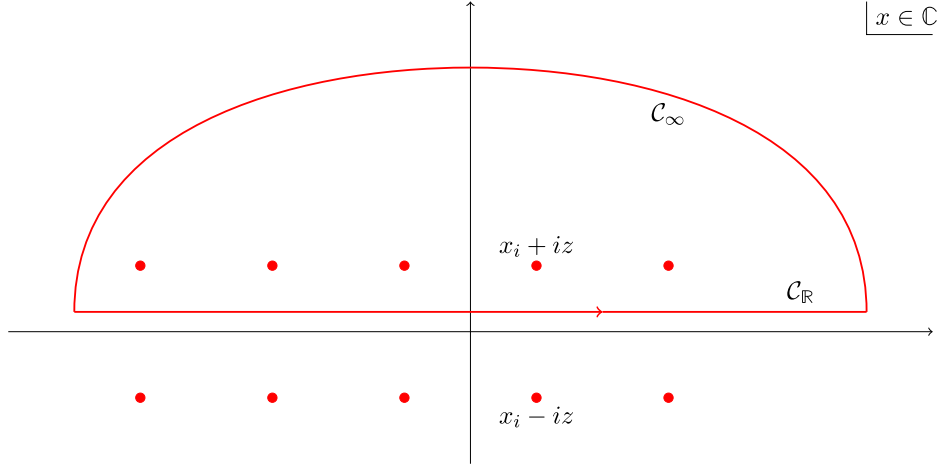[4] For an introduction to the subject, a useful resource is [45].

Figure 2. Contour used for the integral over the variable x parametrising the AdS$_2$ boundary. The contour can be chosen to close in either the upper or lower complex half-plane since the integrand is appropriately bounded at large $|x|$.

3.1. Massless scalar fields

In the case of massless scalar fields, the integral (3.2) reduces to

$$I_{\Delta=1}(x_1,\ldots,x_n) = \int_0^\infty \mathrm{d}z\, z^{n-2} \int_{-\infty}^\infty \mathrm{d}x \frac{1}{\Pi_{i=1}^n (z^2 + (x-x_i)^2)}. \tag{3.4}$$

The advantage of working in AdS$_2$ is that, since the boundary has only one dimension, the integrated boundary coordinate x can be analytically continued to the complex plane and the integral can be evaluated with the residue theorem. The contribution from the contour around infinity ($\mathcal{C}_\infty$ in figure 2) vanishes since the integrand is appropriately bounded at large $|x|$.

The integrand in (3.4) has $2n$ poles at

$$x = x_j \pm \mathrm{i}z, \tag{3.5}$$

where $1 \leqslant j \leqslant n$, with residues

$$\pm \frac{1}{2\mathrm{i}z\Pi_{i\neq j}((x_i - x_j)^2 + 2\mathrm{i}z(x_i - x_j))}, \tag{3.6}$$

which are depicted in figure 2. Since, for $z > 0$, the poles in the upper half-plane (UHP) come with a positive sign and those in the lower half-plane (LHP) come with a minus sign, the result is independent of the choice of closing the contour. However, when z is real, these poles will have an additional factor $\mathrm{sgn}(z)$. This is because the poles cross the $x \in \mathbb{R}$ axis when z crosses 0.

We are thus left with the integral

$$I(x_i) = \pi \int_0^\infty \mathrm{d}z\, z^{n-3} \sum_{j=1}^n \frac{1}{\Pi_{l=1, i\neq j}^n ((x_i - x_j)^2 + 2\mathrm{i}z(x_i - x_j))}. \tag{3.7}$$
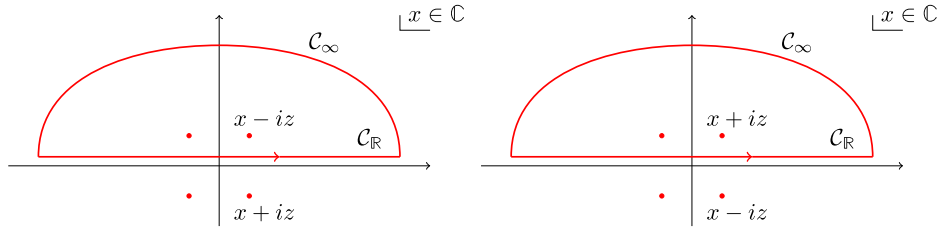
Figure 3. The contour here is closed in the UHP (the same analysis holds for the LHP closing). However, since z is now defined on the entire real line the pole enclosed in the given contour depends on the sign of z. The case where $z < 0$ (left) will have a residue of opposite sign when compared to that where $z > 0$ (right).

The integrand of (3.7) has a leading large z behaviour

$$\pi \sum_{j=1}^{n-1} \frac{z^{-1}}{(2\mathrm{i})^{n-2}} \frac{1}{\prod_{i=1,i\neq j}^n (x_i - x_j)} + O(z^{-2}), \tag{3.8}$$

which vanishes thanks to the identity

$$\sum_{j\in J} \frac{1}{\prod_{i\in J,i\neq j}(x_i - x_j)} = 0, \tag{3.9}$$

so the integral is convergent for $n \geqslant 3$ as expected. Notice that the integrand of (3.7) has the same parity as the number of external fields. This leads to a simplification in computing the odd n-point functions.

n odd.

The massless odd-n case can be solved with contour integration for both the x and the z coordinates[5]. Since both the integrand and the residue of the pole in the x coordinates are antisymmetric under $z \to -z$, we can extend the region of integration of z to the entire real line. This is best seen in the trivial example of the conformal massless three-point function

$$\lim_{\Lambda\to\infty} \Lambda^2 I(0,1,\Lambda) = \int_0^\infty \frac{\mathrm{d}z}{z^2} \int_{-\infty}^\infty \mathrm{d}x \frac{z^3}{(z^2+x^2)(z^2+(x-1)^2)}. \tag{3.10}$$

Since the integrand is antisymmetric under $z \to -z$, we need to compensate for the sign change when extending the range of the integral over z

$$\frac{1}{2}\int_{-\infty}^\infty \frac{\mathrm{d}z\,\mathrm{sgn}(z)}{z^2} \int_{-\infty}^\infty \mathrm{d}x \frac{z^3}{(z^2+x^2)(z^2+(x-1)^2)}. \tag{3.11}$$

When considering the x-contour integral (3.11), we are now faced with two situations for the contour integral, the first ($z < 0$) is depicted on the left of figure 3, the second ($z > 0$) is depicted on the right.

The sign of the pole included in the contour cancels the sign contribution from equation (3.11). The range of z can be extended after having done the x-integral to obtain

---

[5] This is true for any convergent integral with odd $\sum_i \Delta_i$. The resulting correlator will thus be a rational polynomial in the cross-ratios though it may not have a simple form.

the same conclusion. In so doing, one obtains

$$\pi \int_{-\infty}^{\infty} dz \frac{1}{4z^2 + 1} = \frac{\pi^2}{2}. \tag{3.12}$$

This reasoning holds for a general n-point function whose integrand is antisymmetric under $z \to -z$. We will see in one of the examples in section 4, the case of topological operators where the polynomial dependence on the external coordinates is just a constant (up to a sign-dependent factor).

We are then left with an analytic integral over the entire real z-line.

$$I(x_i) = \frac{2\pi i}{2} \int_{-\infty}^{+\infty} dz z^{n-2} \sum_{j=1}^{n-1} \frac{1}{2iz\Pi_{i\neq j}((x_i - x_j)^2 + 2iz(x_i - x_j))} \tag{3.13}$$

$$= \frac{\pi}{2} \int_{-\infty}^{+\infty} dz z^{n-3} \sum_{j=1}^{n-1} \frac{1}{\Pi_{i\neq j}((x_i - x_j)^2 + 2iz(x_i - x_j))}. \tag{3.14}$$

The integrand has a good large-$|z|$ behaviour and we can therefore analytically continue z and evaluate this integral by contour integration, neglecting the vanishing contribution from the contour at ∞. There are poles at positions

$$z^* = -\frac{x_i - x_j}{2i}, \tag{3.15}$$

with residues

$$\text{Res}_{z=z^*}\left(\frac{z^{n-3}}{\Pi_{k\neq j}((x_k - x_j)^2 + 2iz(x_k - x_j))} \right) = \frac{(x_i - x_j)^{n-4}}{(2i)^{n-4}\Pi_{k\neq j\neq i}(x_k - x_j)(x_k - x_i)}. \tag{3.16}$$

We close the contour in the UHP, in which only the poles where $x_i - x_j > 0$ contribute. This gives the final result for odd-n and ordered x_i

$$I_{n\,\text{odd}}(x_i) = \frac{\pi^2}{2(2i)^{n-3}} \sum_{i>j}^{n} \frac{(x_i - x_j)^{n-4}}{\Pi_{k\neq j\neq i}(x_k - x_j)(x_k - x_i)}. \tag{3.17}$$

This formula agrees with the canonical case of $n = 3$, and the explicit results for $n = 5$ and $n = 7$ are given in appendix A.2.

Even and odd n.

For a generic number of external fields n, the integral

$$I(x_i) = \pi \int_0^\infty dz z^{n-3} \sum_{j=1}^{n} \frac{1}{\Pi_{l=1,i\neq j}^{n} ((x_i - x_j)^2 + 2iz(x_i - x_j))}, \tag{3.18}$$

cannot be evaluated with contour integration. It can still be evaluated explicitly with the pole-matched, partial fraction decomposition of the integrand

$$\sum_j \frac{z^{n-3}}{\Pi_{k\neq j}\left(2i(x_k - x_j)\left(z - i\frac{x_k-x_j}{2}\right)\right)} = \frac{1}{(2i)^{n-2}} \sum_{i\neq j} \frac{(x_i - x_j)^{n-4}}{\Pi_{k\neq i\neq j}(x_i - x_k)(x_k - x_j)} \frac{-1}{(z + a_{ij})}, \tag{3.19}$$

where

$$a_{ij} = \frac{x_i - x_j}{2i}. \tag{3.20}$$

Using this decomposition, we obtain logarithm functions whose branch cut is chosen to be on the negative real axis. The choice of the branch of the logarithm is arbitrary since we do not cross any branch cut in the definite integration[6]. The convergent commuting of the sum and the integral is ensured by only taking the upper bound Λ to infinity at the end of computations. This gives the result

$$I(x_i) = \lim_{\Lambda \to \infty} \frac{-\pi}{(2i)^{n-2}} \sum_{i \neq j} \frac{(x_i - x_j)^{n-4}}{\Pi_{k \neq i \neq j}(x_i - x_k)(x_k - x_j)} \big(\ln(a_{ij} + \Lambda) - \ln(a_{ij}) \big), \tag{3.21}$$

which can be simplified by averaging over the permutation of the two indices, since the sum is indiscriminate in i and j. The first consequence is that the divergent term cancels in both cases, since we have

$$\log(\Lambda) \sum_{i \neq j} \frac{(x_i - x_j)^{n-4}}{\Pi_{k \neq i \neq j}(x_i - x_k)(x_j - x_k)} = 0 \quad n \text{ even,} \tag{3.22}$$

and in the odd-n case we have a vanishing leading term since

$$\ln\left(\Lambda - i\frac{x_i - x_j}{2} \right) - \ln\left(\Lambda + i\frac{x_i - x_j}{2} \right) \xrightarrow{\Lambda \to \infty} 0. \tag{3.23}$$

Thus, we can write the result as

$$I(x_i) = \frac{\pi}{(2i)^{n-2}} \sum_{i \neq j} \frac{(x_i - x_j)^{n-4}}{\Pi_{k \neq i \neq j}(x_i - x_k)(x_k - x_j)} \ln\left(\frac{x_i - x_j}{2i} \right), \tag{3.24}$$

which is a real quantity for both the even case

$$I_{\text{even}}(x_i) = \frac{\pi}{2(2i)^{n-2}} \sum_{i \neq j} \frac{(x_i - x_j)^{n-4}}{\Pi_{k \neq i \neq j}(x_i - x_k)(x_j - x_k)} \ln\big((x_i - x_j)^2\big), \tag{3.25}$$

and the odd-n case

$$\begin{aligned}
I_{\text{odd}}(x_i) &= \frac{\pi}{2(2i)^{n-2}} \sum_{i \neq j} \frac{(x_i - x_j)^{n-4}}{\Pi_{k \neq i \neq j}(x_i - x_k)(x_j - x_k)} \big(\ln(a_{ij}) - \ln(-a_{ij}) \big) \\
&= \frac{\pi}{2(2i)^{n-2}} \left(i\pi \sum_{i > j} \frac{(x_i - x_j)^{n-4}}{\Pi_{k \neq i \neq j}(x_i - x_k)(x_j - x_k)} - i\pi \sum_{i < j} \frac{(x_i - x_j)^{n-4}}{\Pi_{k \neq i \neq j}(x_i - x_k)(x_j - x_k)} \right) \\
&= \frac{\pi^2}{2(2i)^{n-3}} \sum_{i > j} \frac{(x_i - x_j)^{n-4}}{\Pi_{k \neq i \neq j}(x_i - x_k)(x_j - x_k)}. \tag{3.26}
\end{aligned}$$

---

[6] The author thanks Luke Corcoran for a discussion on this point.

Thus equation (3.24) is consistent with the result (3.17) found in the previous section. The correlator (3.3) follows from (3.26) and (3.25). This matches known literature for the case of the four-point function

$$I_{\Delta=1,n=4} = -\frac{\pi}{2}\left(\frac{\log(u_1)}{1-u_1} + \frac{\log(1-u_1)}{u_1}\right) \tag{3.27}$$

and more cases are listed in appendix A.2.

3.2. Massive scalar fields

The method used in section 3.1 is very powerful in the generic n case but quickly increases in complexity when $\Delta > 1$. However, another method can be used to obtain the massive n-point functions from the massless cases, as seen below in subsection 3.3.

For $\Delta = 2$, the result can still be computed with this method relatively efficiently. The integral

$$I_{\Delta=2}(x_i) = \int dz z^{2n-2} \int dx \frac{1}{\Pi_{i=1}^{n}(z^2 + (x - x_i)^2)^2} \tag{3.28}$$

is evaluated by contour integration for the $x-$integral and partial fraction decomposition for the $z-$integral. Double poles lead to the less compact formula

$$
I_{\Delta=2,n} = \sum_i \sum_{j\neq i} \frac{-\pi}{2(2\mathrm{i})^{2n-4}(x_i - x_j)^2} \partial_{x_j}\left(\frac{(x_j - x_i)^{2n-5}}{\prod_{k\neq j,k\neq i}(x_k - x_j)^2(x_k - x_i)^2} \ln\frac{x_j - x_i}{2\mathrm{i}}\right)
$$
$$
+ \sum_i \sum_{j\neq i} \partial_{x_i} \frac{-\pi}{(2\mathrm{i})^{2n-2}(x_i - x_j)^2} \partial_{x_j}\left(\frac{(x_j - x_i)^{2n-4}}{\prod_{k\neq j,k\neq i}(x_k - x_j)^2(x_i - x_k)^2} \ln\frac{x_j - x_i}{2\mathrm{i}}\right),
$$
$$\tag{3.29}$$

which is derived in appendix A.1. One expects a similar structure at higher Δ, where we have a double sum over the external coordinates $x_{i,j}$ and $\partial^{2\Delta}$ derivatives and Δ terms. Some evidence of this is the pinching presented in section 3.3 though subtleties in the order of limits prevent a general analysis in this paper. As such, the residue method loses its efficiency as we increase the dimension of the external operators.

3.3. Pinching

One of the ways to relate correlators with differing number of points is through *pinching*, that is, bringing an operator near another

$$\lim_{x_i \to x_{i+1}} \langle \phi(x_1)\ldots\phi(x_i)\phi(x_{i+1})\ldots\phi(x_n)\rangle. \tag{3.30}$$

From the OPE, one expects a divergence in this pinching limit. The contribution from the exchanged identity, in particular, leads to a power divergence

$$\lim_{\epsilon \to 0}\langle\phi_\Delta(x_1)\phi_\Delta(x_1 + \epsilon)\rangle \sim \epsilon^{-2\Delta}. \tag{3.31}$$

Useful results can still be obtained through a similar limit relating not the full correlators but the individual contact diagrams (see figure 4). In particular, the limit of the unit normalised propagators

$$\lim_{x_2 \to x_1} \tilde{K}_{\Delta_1}(x_1; x, z)\tilde{K}_{\Delta_1}(x_1; x, z) = \tilde{K}_{\Delta_1 + \Delta_2}(x_1; x, z) \tag{3.32}$$
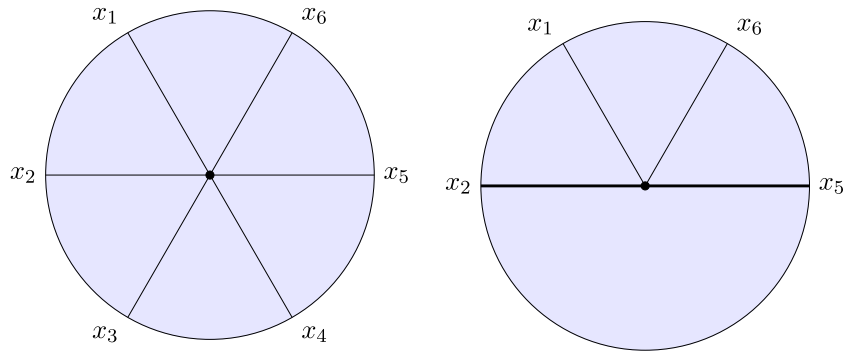
Figure 4. Pinching of the $I_{\Delta=1,n=6}$ integral to $I_{[1,2,2,1]}$ where the thick lines represent $\Delta = 2$ bulk-to-boundary propagators.

indicates that the pinching of operators should relate higher-point integrals to higher-weight integrals if this limit commutes with the integrals considered in this paper.

One expects this commuting between the limit and the integral to break down as soon as one encounters divergences. In other words, in the absence of divergences,

$$\lim_{x_{i+1} \to x_i} I_{[\Delta_1,\dots,\Delta_n]}(x_1,\dots,x_n) = I_{[\Delta_1,\dots,\Delta_i+\Delta_{i+1},\bar{\Delta}_{i+1},\dots,\Delta_n]}(x_1,\dots,\bar{x}_{i+1},\dots,x_n), \tag{3.33}$$

where $\bar{x}_{i+1}$ denotes the absence of an operator at position x_{i+1}. The process can be iterated to form massive contact n-point diagrams from the basis of massless contact diagrams. This can, in principle, be done for all values of Δ and n. A list of examples for scalars of differing dimensions is given in appendix A.2, agreeing with numerical integration and known results. This provides a non-trivial check of the six-point function as well as a way to evaluate the four-point correlator of massive fields. When divergences are present in the individual diagrams, these might cancel in the full correlator, and if not need to be regularised.

The simplest example in which divergences naturally appear in a pinched contact diagram is when considering the pinching from a four- to a three-point function

$$\lim_{x_2 \to x_1} \langle \phi(x_1)\phi(x_2)\phi(x_3)\phi(x_4) \rangle = \lim_{x_2 \to x_1} \left(\frac{1}{x_{13}^2 x_{24}^2} \left(\frac{-2 \log(\chi)}{1-\chi} - \frac{2 \log(1-\chi)}{\chi} \right) \right)$$

$$= \frac{1}{x_{13}^2 x_{14}^2} \lim_{\epsilon \to 0}(-2 \log(\epsilon) - 2), \tag{3.34}$$

where the pinched cross-ratio $\chi \to 0$ generates a divergence in the pinched correlator. In some physical systems, the cancelation of such divergences can occur thanks to the symmetries of the theory. For example, in the pinching of $\mathcal{N} = 4$ fields in [36], the contraction of the R-symmetry indices with a null vector ensures that the protected operators form a chiral ring, and the powers of a single protected operator are still protected. In the generic case where the divergences are retained, these do not necessarily match the corresponding correlator.

From the examples shown in this paper, it seems that the class of scalar contact diagrams follows this general property. In particular, since the dictionary of D-functions is well known, this provides a non-trivial check of the higher-point functions. One would be tempted to apply this pinching to the formal expression (3.24) to have an independent derivation of the $\Delta = 2$ case in (3.29). However, the pinching has to be done after the sum to have consistent limits, which impedes deriving the $\Delta = 2$ case from the massless one.

With this caveat in mind, the n-point contact diagrams of massless scalars can generate all n-point contact diagrams.

4. An application: topological correlators

This example considers non-Abelian gauge theories in AdS$_2$ and is an alternative construction to the Witten diagram computation in appendix A.2 of [34]. For consistency with the notation in [34], we denote the boundary coordinate by t instead of x.

Yang–Mills in AdS$_2$.

We review the setting of [34] where the strong coupling action is that of Yang–Mills theory in AdS$_2$ completed with a regulating boundary term

$$S_{\text{YM}} = \frac{1}{2g_{\text{YM}}^2} \int_{\text{AdS}_2} dx^2 \sqrt{-g} \, \text{Tr}\big(F_{\mu\nu}F^{\mu\nu}\big) \tag{4.1}$$

$$S_{b^y} = \frac{1}{g_{\text{YM}}^2} \int_{\partial\text{AdS}_2} dx \sqrt{-\gamma} \, \text{Tr}\big(A_i A^i - 2A^i F_{\mu i}n^\mu\big), \tag{4.2}$$

where μ, ν are the indices in the bulk coordinates of AdS$_2$, i those of the boundary coordinates, and n^μ is a unit vector normal to the boundary of AdS$_2$.

In radial coordinates, the equation of motion is solved by

$$F_{r\varphi} = Q \sinh r \qquad A_\varphi = Q(\cosh r - 1) \qquad A_r = 0, \tag{4.3}$$

where $Q = Q_a T^a$ is an element of the Lie algebra of the theory and in the following, indices a, b, a_i are those of the gauge algebra. This gives the on-shell action

$$(S_{\text{tot}})_{\text{on-shell}} = -2\pi \frac{\text{Tr}(Q^2)}{g_{\text{YM}}^2}. \tag{4.4}$$

To relate the boundary fields to the bulk fields, the variation of the bulk action needs to be written in terms of the variation of the boundary field

$$\delta S_{\text{tot}} = \frac{2}{g_{\text{YM}}^2} \int_{\partial B} dx \sqrt{-\gamma} \, \text{Tr}\big(A^i \delta a\big) \quad a = \lim_{x^\mu \to \partial B} \big(A_i - F_{\mu i}n^\mu\big), \tag{4.5}$$

where a is thus the corresponding boundary field and i is the index corresponding to the boundary coordinate (t in the following). The on-shell action (4.4) can be written in terms of the boundary fields a through the equation

$$a(\varphi) = -uQu^{-1} + iu\partial_\varphi u^{-1} \tag{4.6}$$

$$u_0 Q u_0^{-1} = \frac{i}{2\pi} \log\left(P \exp\left(i \int_0^{2\pi} d\varphi \, a(\varphi) \right) \right), \tag{4.7}$$

where the φ−dependant large gauge transformations at the boundary are parametrized by u and $P \exp$ denotes the usual path ordered exponential. The expression for the on-shell action is then proportional to the trace of (4.7) squared,

$$\text{Tr}(Q^2) = \text{Tr}((u_0 Q u_0^{-1})^2) = -\frac{1}{4\pi^2}\Omega(a). \tag{4.8}$$

The expression for $\Omega(a)$ is a standard result in quantum mechanics and is solved by the Magnus expansion [46, 47]

$$\exp(\Omega) = P \exp\left(i \int d\varphi a(\varphi)\right). \tag{4.9}$$

This can be used to find the dual correlators through the holographic dictionary

$$\langle j^a(\varphi_1) j^b(\varphi_2) \rangle = \frac{\delta^{ab}}{4\pi g_{YM}^2} \tag{4.10}$$

$$\langle j^a(\varphi_1) j^b(\varphi_2) j^c(\varphi_3) \rangle = -\frac{f^{abc} \operatorname{sgn} \varphi_{12}\varphi_{23}\varphi_{31}}{4\pi g_{YM}^2} \tag{4.11}$$

$$\langle j^{a_1}(\varphi_1) j^{a_2}(\varphi_2) j^{a_3}(\varphi_3) j^{a_4}(\varphi_4) \rangle = -\frac{f^{aa_1 a_2} f^{aa_3 a_4}}{4\pi g_{YM}^2} (\operatorname{sgn} \varphi_{12}\varphi_{24}\varphi_{43}\varphi_{31} - \operatorname{sgn} \varphi_{21}\varphi_{14}\varphi_{43}\varphi_{32})$$

$$+ (2 \leftrightarrow 3) + (2 \leftrightarrow 4), \tag{4.12}$$

where the indices a, b, c, a_i are those of the gauge algebra. Through Witten diagrams, these correlators of boundary terms can be computed explicitly using the contour integral method detailed above. The bulk-to-boundary propagators in Poincaré coordinates for the gauge field A_μ are [20, 48]

$$G_\mu(z, t; t_i) = \frac{z^2 + (t - t_i)^2}{2\pi z} \partial_\mu \left(\frac{t - t_i}{z^2 + (t - t_i)^2}\right), \tag{4.13}$$

or explicitly

$$G_z(z, t; t_i) = \frac{t_i - t}{\pi \left((t - t_i)^2 + z^2\right)} \qquad G_t(z, t, t_i) = \frac{z^2 - (t - t_i)^2}{2\pi z (t - t_i)^2 + z^2}. \tag{4.14}$$

The on-shell action is a pure boundary term

$$S_{on-shell} = \frac{1}{2g_{YM}^2} \int_{AdS_2} dx^2 \sqrt{-g} \operatorname{Tr}\left(D_\mu A_\nu F^{\mu\nu}\right) + \frac{1}{g_{YM}^2} \int_{\partial AdS_2} dx \sqrt{-\gamma} \operatorname{Tr}\left(A_i A^i - 2A^i F_{\mu i} n^\mu\right)$$

$$= \frac{1}{g_{YM}^2} \int_{\partial AdS_2} dx \sqrt{-\gamma} \operatorname{Tr}\left(A_i A^i + A^i F_{i\mu} n^\mu\right). \tag{4.15}$$

Explicitly, in the (z, t) Poincaré coordinates, this gives[7]

$$S_{on-shell} = -\frac{1}{g_{YM}^2} \int dt z \operatorname{Tr}(A_t A_t - z A_t F_{tz})|_{z=0}. \tag{4.16}$$

The two-point correlators are given by Wick contractions acting on this term

$$\langle a^a(t_1) a^b(t_2) \rangle = \lim_{z \to 0} -\frac{1}{2g_{YM}^2} \int dt \delta^{ab} z G_t(z, t, t_2) \left(G_t(z, t; t_1) + z \partial_{[z} G_{t]}(z, t; t_1)\right) \tag{4.17}$$

---

[7] Note that the vector pointing out of the boundary goes in the $-z$ direction.

$$= \lim_{z \to 0} \frac{(t_1 - t_2)^2 \delta^{ab}}{4\pi g_{\text{YM}}^2 \big((t_1 - t_2)^2 + 4z^2\big)} \tag{4.18}$$

$$= \frac{\delta^{ab}}{4\pi g_{\text{YM}}^2}. \tag{4.19}$$

The three-point vertex is

$$S_3 = -\frac{1}{g_{\text{YM}}^2} \int dt \, dz z^2 f_{abc} A_z^a A_t^b \partial_{[z} A_{t]}^c, \tag{4.20}$$

which gives a correlator

$$\langle a^a(t_1) a^b(t_2) a^c(t_3) \rangle = \frac{1}{g_{\text{YM}}^2} \, \text{Perm}\big(f^{abc} I(t_1, t_2, t_3)\big), \tag{4.21}$$

where we define the single-Wick-contracted integral

$$I(t_1, t_2, t_3) = \int dt \, dz z^2 G_z(z, t; t_1) G_t(z, t; t_2) \partial_{[z} G_{t]}(z, t; t_3). \tag{4.22}$$

The anti-symmetrised derivative removes the t_3 dependence, and the parity of this integrand under $z \to -z$ is the same as that of the odd n massless scalar case (see section 3.1) so we can evaluate both the z and t integrals with a complex contour[8]. Extending the z variable to the entire real line we have

$$I(t_1, t_2, t_3) = \int_{-\infty}^{\infty} dt \int_0^{\infty} dz \frac{(t - t_1)\big((t - t_2)^2 - z^2\big)}{4\pi^3 z \big((t - t_1)^2 + z^2\big)\big((t - t_2)^2 + z^2\big)} \tag{4.23}$$

$$= \frac{1}{2} \int_{-\infty}^{\infty} dt \int_{-\infty}^{\infty} dz \, \text{sgn}(z) \frac{(t - t_1)\big((t - t_2)^2 - z^2\big)}{4\pi^3 z \big((t - t_1)^2 + z^2\big)\big((t - t_2)^2 + z^2\big)}. \tag{4.24}$$

This integral has a t_i-independent contribution from the behaviour at $t \to \infty$. However, this is cancelled by the permutation and the antisymmetry of the structure constants. We will therefore ignore this contribution and evaluate the integral by contour integration. The $t-$integral evaluates to

$$I(t_1, t_2, t_3) = \int_{-\infty}^{\infty} \frac{dz}{z} \frac{2z(t_1 - t_2) + i(t_1 - t_2)^2 + 4iz^2}{8\pi^2\big((t_1 - t_2)^2 + 4z^2\big)} \, \text{sgn}(z)^2 \tag{4.25}$$

$$= \int_{-\infty}^{\infty} \frac{dz}{z} \frac{2z(t_1 - t_2) + i(t_1 - t_2)^2 + 4iz^2}{8\pi^2\big((t_1 - t_2)^2 + 4z^2\big)}. \tag{4.26}$$

Just as in the previous case the factors of $\text{sgn}(z)$ cancel and leave an analytic function in z. This integral also has a pole at 0 and at ∞, these can also be cancelled using the antisymmetry of the structure constants of the algebra by considering a combination of Wick contractions; for example $f^{a_1, a_2, a_3}\big(I_{t_1, t_2, t_3} - I_{t_2, t_1, t_3}\big)$. With this in mind, the integral can be evaluated using contour integration. The only remaining pole is at $z = \pm i \frac{t_1 - t_2}{2}$ and therefore the integral will have a factor of $\text{sgn}(t_1 - t_2)$ multiplying the residue at that point (see figure 5).

---

[8] There is a convergence issue in $I(t_1, t_2, t_3)$ which is solved when considering the sum of the Wick contractions, since the leading term is t^{-1}, this is always cancelled by an odd permutation of the indices $(1, 2, 3)$, the next to leading term is convergent.
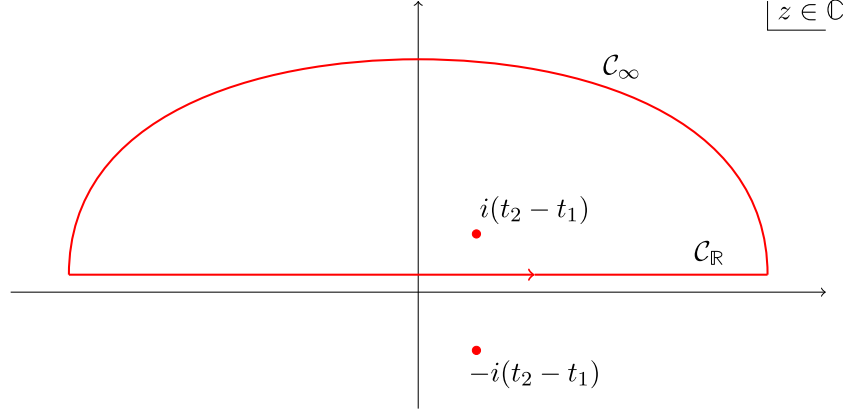
Figure 5. Contour used for the $z-$integral in equation (4.26), the origin of the topological factor $\mathrm{sgn}(t_1 - t_2)$ is clear in this setup. The contour is closed in the UHP (the same analysis holds for the LHP closing). The pole contained within this contour depends on the sign of $(t_1 - t_2)$ where, in this example, we have shown the case $t_1 < t_2$.

This gives the result for one diagram

$$I(t_1, t_2, t_3) = \frac{1}{2\pi} \, \mathrm{sgn}(t_1 - t_2), \tag{4.27}$$

and therefore

$$\langle a^a(t_1) a^b(t_2) a^c(t_3) \rangle = \frac{1}{8\pi g_{\mathrm{YM}}^2} \left(\sum_{\sigma(\{1,2,3\})} (f^{a_1 a_2 a_3} \, \mathrm{sgn}(t_1 - t_2)) \right) \Big|_{\{a_1, a_2, a_3\} \to \{a, b, c\}}. \tag{4.28}$$

Using the total antisymmetry of the structure constants we have

$$\sum_{\sigma(\{1,2,3\})} (f^{a_1 a_2 a_3} \, \mathrm{sgn}(t_1 - t_2)) \big|_{\{a_1, a_2, a_3\} \to \{a, b, c\}} = -2 f^{abc} \, \mathrm{sgn}(t_{12} t_{23} t_{31}), \tag{4.29}$$

which gives the final result

$$\langle a^a(t_1) a^b(t_1) a^c(t_1) \rangle = -\frac{1}{4\pi g_{\mathrm{YM}}^2} f^{abc} \, \mathrm{sgn}(t_{12} t_{23} t_{31}). \tag{4.30}$$

This agrees with the result for the topological three-point function seen above through a simple change of coordinates[9].

5. Exchanges and Polyakov blocks

Exchange diagrams immediately increase the difficulty of the calculation by adding a bulk integration as well as a bulk-to-bulk propagator. For example, the t-channel exchange diagram

---

[9] For higher-point functions, there is the subtlety that the boundary field a is not the boundary limit of the gauge field A_μ, but rather has a dependence on both A_μ and $F_{\mu\nu}$. This implies that the bulk-to-boundary propagator receives corrections from multi-source terms. These questions are addressed in [34] but are beyond the scope of this paper.

is given by the integral

$$J(x_1, \ldots, x_4) = \int \frac{\mathrm{d}^2 z_a}{z_{a,0}^2} I(z_a, x_2, x_3) K_{\Delta_1}(x_1, z_a) K_{\Delta_4}(x_4, z_a) \tag{5.1}$$

$$I(w, x_2, x_3) = \int \frac{\mathrm{d}^2 z}{z_0^2} G_{\Delta_{\mathrm{E}}}(w, z) K_{\Delta_2}(x_2, z) K_{\Delta_3}(x_3, z), \tag{5.2}$$

where K_Δ and $G_{\Delta_{\mathrm{E}}}$ are defined in equation (2.23) and $z_a = (z_{a,0}, z_{a,1})$ are bulk coordinates. Using the isometries of AdS space, the exchange diagrams can be related to contact diagrams [22, 33] such as those presented in section 3.1. This toy example is slightly different to the case in [22], since the sum of contact diagrams does not truncate, but allows for an explicit example of a non-vanishing Polyakov block. Since both bulk integrations in the exchange Witten diagram integral have conformal symmetry, the solution is invariant under the action of symmetry generators on the legs attached to each of the bulk points

$$(\mathcal{L}_a + \vec{L}_2 + \vec{L}_3) I(z_a, x_a; x_2, x_3) = 0. \tag{5.3}$$

This allows one to relate the quadratic Casimir acting on the external legs to the Laplacian acting on the corresponding bulk point

$$(C_{(23)}^{(2)} - m_{\mathrm{E}}^2) I(z_a, x_a; x_2, x_3) = \int \frac{\mathrm{d}^2 z}{z_0^2} \big((\nabla_a^2 - m_{\mathrm{E}}^2) G_{\Delta_{\mathrm{E}}}(w, z) \big) K_{\Delta_2}(x_2, z) K_{\Delta_3}(x_3, z). \tag{5.4}$$

Given that the bulk-to-bulk propagator satisfies the equation of motion, this term in (5.4) reduces to a delta function, thus reducing the number of integrals. The problem is then more tractable since the double AdS$_2$ bulk integrations are replaced by a differential equation relating the answer to the known case of contact diagrams[10], which is a single bulk integral.

Let us now consider a $\lambda \phi^3$ interaction in AdS$_2$ which gives a non-vanishing three-point function and an exchange diagram for the four-point function. For the case of four-point correlators, the exchange diagram integral is solved explicitly in the s, t and u channels.

$$\langle \phi(x_1) \phi(x_2) \phi(x_3) \phi(x_4) \rangle = \frac{\lambda^2 C_\Delta^4 C_{\Delta_{\mathrm{E}}}}{(x_{13} x_{24})^2} \left(f_t^{\Delta, \Delta_{\mathrm{E}}}(z) + f_s^{\Delta, \Delta_{\mathrm{E}}}(z) + f_u^{\Delta, \Delta_{\mathrm{E}}}(z) \right), \tag{5.5}$$

where C_Δ is the normalisation defined in equation (2.22). For example in the t channel,

$$(C_{(23)}^{(2)} - \Delta_{\mathrm{E}}(\Delta_{\mathrm{E}} - 1)) \frac{1}{(x_{13} x_{24})^{2\Delta_\phi}} f_t^{\Delta, \Delta_{\mathrm{E}}}(z) = \frac{1}{(x_{13} x_{24})^{2\Delta_\phi}} I_{\Delta, n=4}(z), \tag{5.6}$$

where $C_{(23)}^{(2)}$ is the quadratic Casimir acting on the external points 2 and 3, Δ_{E} is the conformal dimension of the exchanged operator, $f_t^{\Delta, \Delta_{\mathrm{E}}}$ is the function of the cross-ratio z corresponding to the Witten exchange diagram in the t-channel ($J(x_1, \ldots, x_4)$ in equation (5.1)), and $I_{\Delta, n=4}$ is the contact integral defined in (3.2). For more details in the derivation and the computation, see appendix B.2. In one dimension, this differential equation simplifies to one of a single variable

$$\big((z-1) \big((z-1) z f''(z) + (4\Delta z + z - 1) f'(z) \big) + f(z)(2\Delta(2\Delta z - 1) - m_{\mathrm{E}}) \big) = I_{\Delta, n=4}(z). \tag{5.7}$$

---

[10] A more detailed review of the derivation is presented in appendix B.2.

And can be solved for example for $\Delta_\phi = \Delta_{\text{exch}} = 1$

$$f_t^{(1,1)}(z) = \frac{\pi}{4} \frac{c_1 + c_2 \log(z^2) + 6\text{Li}_3(z) - \text{Li}_2(z)\log(z^2)}{(z-1)^2}. \tag{5.8}$$

The same can be done in the other channels; in the s-channel, we have

$$f_s^{(1,1)}(z) = \frac{\pi}{4} \frac{c_1 + c_2 \log((1-z)^2) + 6\text{Li}_3(1-z) - \text{Li}_2(1-z)\log((1-z)^2)}{z^2} \tag{5.9}$$

$$= f_t^{(1,1)}(1-z). \tag{5.10}$$

In the u-channel, we have

$$f_u^{(1,1)}(z) = \frac{\pi}{4}\left(c_3 + 6\text{Li}_3\left(\frac{z}{z-1}\right) - \text{Li}_2\left(\frac{z}{z-1}\right)\log\left(\left(\frac{z}{1-z}\right)^2\right) + c_4 \log\left(\left(\frac{z}{1-z}\right)^2\right) \right)$$

$$= (1-z)^{-2} f_t\left(\frac{z}{z-1}\right). \tag{5.11}$$

The symmetry of the three channels is clear: the s and t channels are related by $z \to 1-z$ crossing which equates their integration constants. The solution which is crossing-symmetric and makes the OPE expansion consistent[11] has the integration coefficients equal to

$$c_1 = c_3 = 6\zeta(3) \tag{5.12}$$

$$c_2 = c_4 = -\frac{\pi^2}{6}. \tag{5.13}$$

Additionally, this solution has the mildest Regge growth.

We can then define the correlator from the sum of the exchanges in the different channels.

$$\langle \phi(x_1)\phi(x_2)\phi(x_3)\phi(x_4) \rangle = \frac{\lambda^2}{\pi^5 (x_{13}x_{24})^2}\left(f_t^{\Delta,\Delta_E}(z) + f_s^{\Delta,\Delta_E}(z) + f_u^{\Delta,\Delta_E}(z) \right). \tag{5.14}$$

The sum of exchanged Witten diagrams can be related to the Polyakov block [39], for an exchanged weight $\Delta = 1$ and external weights $\Delta_\phi = 1$,

$$P_{1,1}^{(0)}(z) = \frac{4}{\pi}\left(f_u^{(1,1)}(z) + f_t^{(1,1)}(z) + f_s^{(1,1)}(z) \right). \tag{5.15}$$

Notice that the u and t channels evaluated in the $\frac{z}{1-z}$ variable are well defined on the analytic continuation to the interval $0 < z < 1$.

$$f_u(z) = (1-z)^{-2} f_t\left(\frac{z}{z-1}\right) \tag{5.16}$$

$$f_t(z) = (1-z)^{-2} f_u\left(\frac{z}{z-1}\right). \tag{5.17}$$

---

[11] The full analysis requires the three-point diagram and is done in appendix B.2.

Due to this 'pseudo-braiding' and crossing properties of this analytically continued function, the double-discontinuity defined in [39] and reviewed in (2.14), can be evaluated quite easily as

$$\text{dDisc}^{(+)}[P_{(1,1)}(z)] = \frac{2G_{h=1}(z)}{z^2}. \tag{5.18}$$

This is the discontinuity in the *s*-channel of the corresponding Polyakov block [39]. Additionally, the bosonic continuation defined via (2.11) is fully symmetric under $s \to t$ and $s \to u$, and is Regge-bounded. Therefore, $P_{1,1}^{(0)}$ in (5.15) is the Polyakov block (defined on $0 < z < 1$) with external weight $\Delta = 1$ and exchanged weight $\Delta_{\text{E}} = 1$,

$$
\begin{aligned}
P_{1,1}^{(0)}(z) = &\, \text{Li}_2\left(\frac{z}{z-1}\right) \log\left(\frac{z^2}{(z-1)^2}\right) - 6\text{Li}_3\left(\frac{z}{z-1}\right) \\
&- \frac{1}{6}\pi^2 \log\left(\frac{z^2}{(z-1)^2}\right) + 6\zeta(3) \\
&+ \frac{\text{Li}_2(1-z)\log\left((z-1)^2\right) - 6\text{Li}_3(1-z) - \frac{1}{6}\pi^2 \log\left((z-1)^2\right) + 6\zeta(3)}{z^2} \\
&+ \frac{\text{Li}_2(z)\log\left(z^2\right) - 6\text{Li}_3(z) - \frac{1}{6}\pi^2 \log\left(z^2\right) + 6\zeta(3)}{(z-1)^2}.
\end{aligned}
\tag{5.19}
$$

This agrees with the computation[12] done via the conformal bootstrap in [10]. Similarly, higher exchanged weights or external weights can be computed, see appendix B.2. Along with constraints from the double-discontinuity and a suitable ansatz, this method might provide a way to compute all Polyakov blocks $P_{1,\Delta_{\text{E}}}^{(0)}(z)$.

Acknowledgments

Data availability statement

All data that support the findings of this study are included within the article (and any supplementary files).

---

[12] We thank Pietro Ferrero for sharing results relating to [10] allowing for a verification of this result.

Appendix A. *n*-point contact integrals

This appendix compiles the derivation of the $\Delta = 2n$-point contact integral, a non-exhaustive list of *n*-point *D*-functions, and a short numerical analysis of the results obtained for a large number of external legs.

A.1. Derivation of $\Delta = 2$

One may of course be interested in higher Δ. This is where this method loses some of its power. While it is very powerful in the generic *n* regime, it quickly increases in complexity when Δ is increased. However, the complexity will only be combinatorial and not intrinsic. The integrand of

$$I(x_i) = \int \mathrm{d}z z^{2n-2} \int \mathrm{d}x \frac{1}{\prod_{i=1}^{N-1}(z^2 + (x - x_i)^2)^2}, \tag{A.1}$$

only has double poles (and single poles from the expansion around these poles), at the position $x = x_i + \mathrm{i}z$ with residue

$$\operatorname*{Res}_{x=x_i+\mathrm{i}z}\left(\frac{1}{\prod(z^2 + (x-x_i)^2)^2}\right) = \partial_x\left(\frac{1}{(x-(x_i-\mathrm{i}z))^2}\frac{1}{\prod_{j,j\neq i}(z^2+(x-x_j)^2)^2}\right)\Bigg|_{x=x_i+\mathrm{i}z} \tag{A.2}$$

$$= -\sum_i \frac{1}{4z^2}\left(\frac{1}{\mathrm{i}z} + \partial_{x_i}\right)\left(\frac{1}{\prod_{j\neq i}(x_i - x_j)^2(2\mathrm{i}z + (x_i - x_j))^2}\right),$$

where the residue was massaged into a more useable form. As is the massless case, these can be integrated by using the partial fraction decomposition. By comparison of simple and double poles we have

$$\sum_i \frac{z^{2n-n_0}}{\prod_k (z + a_{ik})^2} = \sum_{i\neq j}\frac{c_{ij}}{(z+a_{ij})^2} - \sum_{i\neq j}\frac{\partial_{a_{ij}}c_{ij}}{(z+a_{ij})} \tag{A.3}$$

$$= -\sum_{i\neq j}\partial_{a_{ij}}\left(\frac{c_{ij}}{(z+a_{ij})}\right), \tag{A.4}$$

$$c_{ij} = \frac{(-a_{ij})^{2n-n_0}}{\prod_{k\neq j}(a_{ki} - a_{ji})^2}. \tag{A.5}$$

as long as the $n_0 > -1$. This is integrated by sight

$$\int_0^\Lambda \mathrm{d}z\left(\sum_{i\neq j}\frac{c_{ij}}{(z+a_{ij})^2} - \sum_i \frac{\partial_{a_{ij}}c_{ij}}{(z+a_{ij})}\right) = \sum_{i\neq j}\partial_{a_{ij}}\left(c_{ij}\ln(a_{ij})\right) + (\partial_{a_i}c_{ij})\ln(\Lambda). \tag{A.6}$$

Explicitly, we have

$$\int \mathrm{d}z z^{2n-2}\frac{-1}{4z^2}\sum_i \partial_{x_i}\left(\frac{1}{\prod_{j\neq i}(x_i - x_j)^2(2\mathrm{i}z + (x_i - x_j))^2}\right) \tag{A.7}$$

$$= \sum_i \sum_{j\neq i}\partial_{x_i}\frac{1}{4(2\mathrm{i})^{2n-3}(x_i - x_j)^2}\partial_{x_j}\left(\frac{(x_j - x_i)^{2n-4}}{\prod_{k\neq j,k\neq i}(x_k - x_j)^2(x_i - x_k)^2}\ln\frac{x_j - x_i}{2\mathrm{i}}\right), \tag{A.8}$$

and

$$\int dz \frac{z^{2n-5}}{4i} \left(\frac{1}{\prod_{j \neq i}(x_i - x_j)^2 (2iz + (x_i - x_j))^2} \right)$$

$$= \sum_i \sum_{j \neq i} \frac{1}{4i(2i)^{2n-4}(x_i - x_j)^2} \partial_{x_j} \left(\frac{(x_j - x_i)^{2n-5}}{\prod_{k \neq j, k \neq i}(x_k - x_j)^2 (x_k - x_i)^2} \ln \frac{x_j - x_i}{2i} \right). \quad (A.9)$$

As in the massless case, the divergent terms cancel and the logarithm is a well-defined function with a branch cut on the negative real axis. This gives the result

$$I_{\Delta=2,n}(x_i) = \sum_i \sum_{j \neq i} \frac{-\pi}{2(2i)^{2n-4}(x_i - x_j)^2} \partial_{x_j} \left(\frac{(x_j - x_i)^{2n-5}}{\prod_{k \neq j, k \neq i}(x_k - x_j)^2 (x_k - x_i)^2} \ln \frac{x_j - x_i}{2i} \right)$$

$$+ \sum_i \sum_{j \neq i} \partial_{x_i} \frac{-\pi}{(2i)^{2n-2}(x_i - x_j)^2} \partial_{x_j} \left(\frac{(x_j - x_i)^{2n-4}}{\prod_{k \neq j, k \neq i}(x_k - x_j)^2 (x_i - x_k)^2} \ln \frac{x_j - x_i}{2i} \right).$$

$$(A.10)$$

A.2. Library of contact correlators

In the main body, results are naturally written in terms on the cross-ratios u_i defined in equation (2.5). However, they also hold for the external coordinates, for example $\{x_1, \dots, x_4\}$ combine naturally to form the cross-ratio u_1 in (3.27) in the case of the four-point function

$$I_{\Delta=1,n=4}(x_1, \dots, x_4)$$

$$= -\frac{\pi}{2} \left(\frac{\log x_{12}}{x_{23}x_{13}x_{24}x_{14}} + \frac{\log x_{13}}{x_{12}x_{23}x_{34}x_{14}} + \frac{\log x_{23}}{x_{12}x_{13}x_{34}x_{24}} \right.$$

$$\left. + \frac{\log x_{34}}{x_{13}x_{23}x_{14}x_{24}} + \frac{\log x_{24}}{x_{12}x_{23}x_{14}x_{34}} + \frac{\log x_{14}}{x_{12}x_{13}x_{24}x_{34}} \right)$$

$$= -\frac{\pi}{2(x_{13}x_{24})^2} \left(\frac{x_{13}x_{24}}{x_{14}x_{23}} \log\left(\frac{x_{12}x_{34}}{x_{13}x_{24}} \right) + \frac{x_{13}x_{24}}{x_{12}x_{34}} \log\left(\frac{x_{14}x_{23}}{x_{13}x_{24}} \right) \right). \quad (A.11)$$

Below, we include a few examples $I(0, u_1, \dots, u_{n-3}, 1, \infty)$ of the contact integral (3.2) evaluated in the cross-ratios defined in (2.5), where we use the notation $I_{\Delta,n}$ for equal dimension operators and $I_{[\Delta_1,\dots,\Delta_n]}$ to include external operators of different dimensions.

$$I_{1,3} = \frac{\pi^2}{2} \quad (A.12)$$

$$I_{1,4} = -\frac{\pi}{2} \left(\frac{\log(u_1)}{1 - u_1} + \frac{\log(1 - u_1)}{u_1} \right) \quad (A.13)$$

$$I_{1,5} = \frac{\pi^2}{4u_2(1 - u_1)} \quad (A.14)$$

$$I_{1,6} = \frac{\pi}{8} \left(\frac{(u_1 - 1)^2 \log(1 - u_1)}{u_1(u_1 - u_2)(u_2 - 1)(u_1 - u_3)(u_3 - 1)} \right.$$

$$+ \frac{(u_1 - u_2)^2 \log(u_2 - u_1)}{(u_1 - 1)u_1(u_2 - 1)u_2(u_1 - u_3)(u_2 - u_3)}$$

$$- \frac{(u_2 - 1)^2 \log(1 - u_2)}{(u_1 - 1)(u_1 - u_2)u_2(u_2 - u_3)(u_3 - 1)}$$

$$+ \frac{u_2^2 \log(u_2)}{u_1(u_1 - u_2)(u_2 - 1)(u_2 - u_3)u_3}$$

$$+ \frac{(u_3 - 1)^2 \log(1 - u_3)}{(u_1 - 1)(u_2 - 1)(u_1 - u_3)(u_2 - u_3)u_3}$$

$$+ \frac{(u_2 - u_3)^2 \log(u_3 - u_2)}{(u_1 - u_2)(u_2 - 1)u_2(u_1 - u_3)(u_3 - 1)u_3}$$

$$- \frac{(u_1 - u_3)^2 \log(u_3 - u_1)}{(u_1 - 1)u_1(u_1 - u_2)(u_2 - u_3)(u_3 - 1)u_3}$$

$$- \frac{u_3^2 \log(u_3)}{u_1 u_2(u_1 - u_3)(u_2 - u_3)(u_3 - 1)}$$

$$\left. - \frac{u_1^2 \log(u_1)}{(u_1 - 1)(u_1 - u_2)u_2(u_1 - u_3)u_3} \right) \tag{A.15}$$

$$I_{1,7} = \frac{\pi^2}{16(u_1 - 1)(u_2 - 1)u_2(u_1 - u_3)(u_3 - 1)u_3(u_1 - u_4)(u_2 - u_4)u_4}$$

$$\times \left((u_2 - 1)(u_3 - 1)(u_2 - u_4)u_1^2 \right.$$

$$\times + u_2 \left(u_3^2 + u_4(u_3 + u_4 - 2)u_3 - u_4 - u_2(u_3 - 1)(u_3 + u_4 + 1) \right) u_1$$

$$\times + u_2 \left(u_2(u_3 - 1)(u_3 + (u_3 + 1)u_4) - u_3 \left(u_3 \left(u_4^2 + u_4 + 1 \right) - 3u_4 \right) \right) \right). \tag{A.16}$$

For the massive cases, we find agreement between the result of pinching and that of the formula (3.29) which gives for the first few cases:

$$I_{2,3} = \frac{3\pi}{8} \tag{A.17}$$

$$I_{2,4} = -\frac{\pi((\chi - 1)\chi + 1)}{8(\chi - 1)^2 \chi^2} - \frac{\pi \left(2\chi^2 + \chi + 2 \right) \log(1 - \chi)}{16\chi^3} + \frac{\pi(\chi(2\chi - 5) + 5) \log(\chi)}{16(\chi - 1)^3} \tag{A.18}$$

$$I_{2,5} = \frac{\pi}{32} \left(\vphantom{\frac{a}{b}} \right.$$

$$+ \frac{(u - v)^2 \left(u^3(2v - 1) + u^2(3(v - 2)v + 2) + uv(2(v - 3)v + 3) - (v - 2)v^2 \right) \log(v - u)}{(u - 1)^3 u^3 (1 - v)^3 v^3}$$

$$+ \frac{(v - 1)^2 \left(u^2(-(v(2v + 3) + 2)) + u(v + 1)(v(v + 5) + 1) - v(v(2v + 3) + 2) \right) \log(1 - v)}{(u - 1)^3 v^3 (u - v)^3}$$

$$+ \frac{(u-1)^2\big((u(2u+3)+2)v^2 - (u+1)(u(u+5)+1)v + u(u(2u+3)+2)\big)\log(1-u)}{u^3(v-1)^3(u-v)^3}$$

$$+ \frac{v^2\big(7u^2 - (u+1)v^3 + (u+2)(2u+1)v^2 - 7u(u+1)v\big)\log(v)}{u^3(v-1)^3(u-v)^3}$$

$$+ \frac{u^2\big(u^3(v+1) - u^2(v+2)(2v+1) + 7uv(v+1) - 7v^2\big)\log(u)}{(u-1)^3v^3(u-v)^3}$$

$$+ \frac{-2u^4((v-1)v+1) + u^3\big(2v^3 + v^2 + v + 2\big) - 2v^2((v-1)v+1)}{2(u-1)^2u^2(v-1)^2v^2(u-v)^2}$$

$$+ \frac{u\big(-2v^4 + v^3 - 6v^2 + v - 2\big) + v\big(2v^3 + v^2 + v + 2\big)}{2(u-1)^2u(v-1)^2v^2(u-v)^2}\Bigg). \tag{A.19}$$

From pinching, we define the integral with the pinched weights at positions x_i, e.g $I_{[1,2,2,1]}$

$$I_{[2,2,2]} = \frac{3\pi}{8} \tag{A.20}$$

$$I_{[1,1,1,2]} = \frac{\pi^2}{4x_{13}x_{14}x_{24}^2x_{34}} \tag{A.21}$$

$$I_{[2,2,1,1]} = -\frac{\pi(\chi+2)\log(1-\chi)}{8\chi^3} + \frac{\pi}{8\chi^2(1-\chi)} + \frac{\pi\,\log(\chi)}{8(\chi-1)^2} \tag{A.22}$$

$$I_{[2,1,2,1]} = -\frac{(2\pi\chi+\pi)\log(1-\chi)}{8\chi^2} + \frac{\pi}{8(\chi-1)\chi} + \frac{\pi(2\chi-3)\log(\chi)}{8(\chi-1)^2} \tag{A.23}$$

$$I_{[1,2,2,1]} = \frac{\pi\,\log(1-\chi)}{8\chi^2} + \frac{\pi}{8(\chi-1)^2\chi} - \frac{\pi(\chi-3)\log(\chi)}{8(\chi-1)^3} \tag{A.24}$$

$$I_{[2,2,2,1]} = \frac{\pi^2}{8\chi(1-\chi)} \tag{A.25}$$

$$I_{[3,1,2,1]} = \frac{3\pi^2}{16\chi} \tag{A.26}$$

$$I_{[1,2,1,1,1]} = -\frac{\pi v^2\,\log(v)}{8u^2(v-1)(u-v)^2} + \frac{\pi(u(u-2v+2)-v)\log(1-u)}{8u^2(v-1)(u-v)^2}$$

$$+ \frac{\pi(v-u(u+2v-2))\log(v-u)}{8(u-1)^2u^2(v-1)v}$$

$$- \frac{\pi\big(u^2-2u(v+1)+3v\big)\log(u)}{8(u-1)^2v(u-v)^2} + \frac{\pi(v-1)^2\,\log(1-v)}{8(u-1)^2v(u-v)^2} \tag{A.27}$$

$$I_{[2,1,1,2,1]} = -\frac{\pi^2(2uv+u-3v)}{16(u-1)^2v^2} \tag{A.28}$$

$$I_{[1,1,1,1,2,1]} = \frac{\pi^2\big(u_1^2(u_2-1)^2 + u_2(u_2+(2u_2-3)u_3) + u_1u_2(2u_3 - u_2(u_3+2)+1)\big)}{16(u_1-1)^2(u_2-1)^2u_2(u_1-u_3)u_3}. \tag{A.29}$$

There are also some divergent cases

$$I_{[2,1,1]} = \frac{\pi}{2}(1 - \log(\epsilon)) \tag{A.30}$$

$$I_{[1,3,1,1]} = \frac{5\pi}{16(\chi - 1)^2\chi^2} - \frac{\pi((\chi - 3)\chi + 3)\log(\chi)}{8(\chi - 1)^3\chi^2} + \frac{\pi(\chi^2 + \chi + 1)\log(1 - \chi)}{8(\chi - 1)^2\chi^3}$$
$$- \frac{3\pi\log(\epsilon)}{8(\chi - 1)^2\chi^2}. \tag{A.31}$$

We also find agreement between the pinching of the $2n$-point function of massless correlators and the n-point function of $\Delta = 2$ correlators up to $n = 8$, but these were omitted from the text since they are bulky and not elucidating. Notice that the prefactor (2.8) has no neighbouring terms of type $x_{i,i+1}$ except for the $x_{n-1,n}$ term and the $n = 3$ cases, so no single pinching will lead to divergences in the prefactor. In general, one expects the divergences appearing in the pinching to be physical divergences which need to be considered and not artefacts of this method.

A.3. Numerical and analytical agreement

An additional check for the validity of these results is to perform a numerical integration of these quantities for various values of n. This is done through fixing all but one parameter, for example considering the numerical integration of

$$I_{\Delta,n}(0, \chi, 1, 2, \ldots, n - 2) = \int dz\, dx \left(\frac{z}{(z^2 + (x - \chi)^2)}\right)^{\Delta} \prod_{k=0}^{n-2} \left(\frac{z}{(z^2 + (x - k)^2)}\right)^{\Delta}, \tag{A.32}$$

where χ is a free parameter which allows us to compare (A.32) to the analytic results in (3.24). The difference between the two can be seen in figure 6 and shows good agreement for $3 < n < 30$. In the figure, the normalised average over values in $0 < \chi < 1$ of the difference between (A.32) and the analytic result (3.24) is plotted for varying numbers n of external operators.

A second check of validity can be made through analytical comparisons with known results. The results for $n = 3$ and $n = 4$ are well known but become sparser as n grows larger, however, pinching also provides a way to compare higher—n results to higher—Δ four-point correlators, this is done in appendix A.2.

Appendix B. Exchange diagrams

This appendix contains complementary material relating to the derivation and interpretation of the exchange diagrams. First, details on the conformal Casimir and its relation to the equation of motion in AdS are given. Then the derivation of the relation between exchange diagrams and contact diagrams from [26, 33] is reviewed. This is then applied to the toy model of ϕ^3 interaction in AdS$_2$, which gives insight into Polyakov blocks whose perturbative strong coupling structure is shown explicitly

Quadratic Casimir.

The n-Casimir of the boundary conformal group is given by

$$C^{(n)}_{i_1..i_n} = \frac{1}{2}\left\{\sum_{k=1}^{n} L^{(0)}_{i_k}, \sum_{k=1}^{n} L^{(0)}_{i_k}\right\} - \frac{1}{2}\left[\sum_{k=1}^{n} L^{-\alpha}_{i_k}, \sum_{k=1}^{n} L^{\alpha}_{i_k}\right], \tag{B.1}$$

Figure 6. The quantity plotted (for clarity on a logarithmic scale) $\text{Av} = \left\langle \frac{I_n - I_{n,\text{num}}}{I_n} \right\rangle$ is the weighted difference between the numerical integration $I_{\Delta=1,n}$ in equation (A.32) and the corresponding analytical result, averaged over $0 < \chi < 1$ for a number of external points ranging from $n = 3$ to $n = 17$. For this range, the leading error comes from the machine precision in the integral near the endpoints and thus is of the same order for $n = 3$ and $n = 17$. For higher n, the numerical stability of the integral becomes problematic and the numerical results should not be trusted.

where $L^{(0)}$ are elements of the Cartan and the others are the simple roots. Explicitly for a $d = 1$ conformal boundary the differential expression of the operators is:

$$D = L_0 = \Delta + x\partial_x \quad P = L_{-1} = -\partial_x \quad K = L_{+1} = -2\Delta x - x^2\partial_x. \tag{B.2}$$

This leads to a linear Casimir

$$C_a^{(1)} = \Delta(\Delta - 1), \tag{B.3}$$

which is the mass-squared of the bulk operator, and a quadratic Casimir:

$$C_{x,y}^{(2)} = 2(x - y)(-\Delta_1\partial_y + \Delta_2\partial_x) - (y - x)^2\partial_x\partial_y + (\Delta_1 + \Delta_2 - 1)(\Delta_1 + \Delta_2). \tag{B.4}$$

The quadratic Casimir of the AdS_2 isometries is the Laplacian of AdS, this is best seen in flat embedding coordinates where the generators are given by

$$J_{AB} = -\mathrm{i}(X_A\partial_B - X_B\partial_A), \tag{B.5}$$

where $X_A X^A = 1$. The quadratic Casimir of the AdS isometries in embedding coordinates is then

$$-\frac{1}{2}\mathcal{L}_a\mathcal{L}^a = -\frac{1}{2}J_{AB}J^{AB} \tag{B.6}$$

$$= \frac{1}{2}(X_A\partial_B - X_B\partial_A)(X^A\partial^B - X^B\partial^A) \tag{B.7}$$

$$= X_A X^A\partial_B\partial^B + (1 - d)X_B\partial^B \tag{B.8}$$
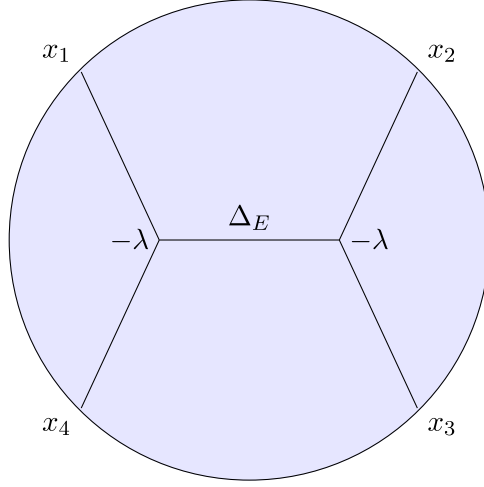
$$= \partial_A\partial^A, \tag{B.9}$$

Figure 7. Exchange Witten diagram for four external insertions of identical scalars of weight Δ_ϕ exchanging a scalar of weight Δ_E in the t channel.

which is the coordinate-independent Laplacian.

A case of interest in this paper is when we have $\Delta_1 = \Delta_2$. The conformal quadratic Casimir then simplifies further to

$$C_z^{(2)} = 2\Delta(2\Delta - 1)f(z) - z\big((z-1)zf''(z) + (2\Delta(z-2) + z)f'(z)\big), \quad \text{(B.10)}$$

where we have made a change of variable

$$z = 1 - \frac{x}{y}. \quad \text{(B.11)}$$

Such changes of variables can be made to reduce this differential equation into a single variable differential equation for each of the (s, t, u) exchange channels.

B.1. Relating the exchange and contact diagrams

We review the analysis from [22, 25], which goes through a detailed computation of the exchange diagram and the z integral. However, they specialise in the case where the resulting exchange correlator can be written in terms of a finite sum of D-functions. The toy model considered in this paper does not satisfy the conditions needed for such a simplification, but still is useful to illustrate the Polyakov blocks.

The integral we are interested in, corresponding to the Witten diagram (figure 7), is

$$J^{(t)}(x_1, \ldots, x_4) = \int \frac{\mathrm{d}^2 w}{w_0^2} I(w, x_2, x_3) K_{\Delta_1}(x_1, w) K_{\Delta_4}(x_4, w), \quad \text{(B.12)}$$

$$I(w, x_2, x_3) = \int \frac{\mathrm{d}^2 z}{z_0^2} G_{\Delta_E}(w, z) K_{\Delta_2}(x_2, z) K_{\Delta_3}(x_3, z). \quad \text{(B.13)}$$

The integral $I(z_a, x_a; \ x_2, x_3)$ is a boundary–boundary-to-bulk three-point function and has conformal symmetry (figure 8).
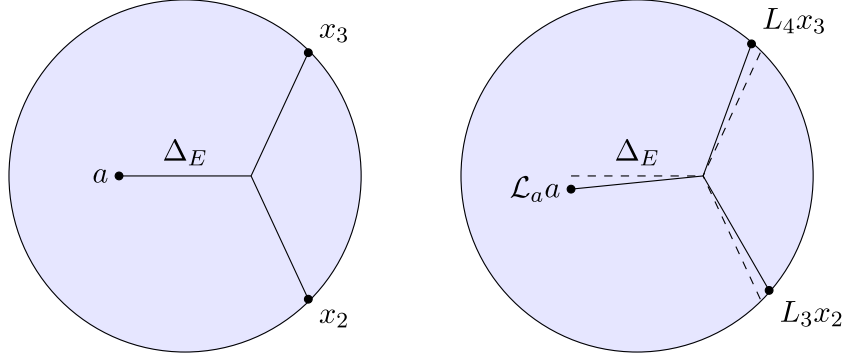
Figure 8. The system is invariant under an infinitesimal transformation (B.14).

$I(w, x_2, x_3)$ in (B.13) is invariant under global transformations generated by $\mathcal{L}_a + \vec{L}_2 + \vec{L}_3$,[13] where the first term generates the isometries of AdS$_2$ and the other two generate the conformal transformation of the boundary. As such, we can write

$$(\mathcal{L}_a + \vec{L}_2 + \vec{L}_3)I(z_a, x_a; x_2, x_3) = 0, \tag{B.14}$$

and can therefore relate the Casimirs of the generators

$$-\frac{1}{2}\mathcal{L}_a^2 I(z_a, x_a; x_2, x_3) = -\frac{1}{2}(\vec{L}_2 + \vec{L}_3)^2 I(z_a, x_a; x_2, x_3) \tag{B.15}$$

$$= C_2^{(23)}I(z_a, x_a; x_2, x_3). \tag{B.16}$$

In one dimension, the quadratic Casimir of the AdS$_2$ isometries is the Laplacian of the bulk appendix B. This Laplacian will allow us to get rid of the bulk-to-bulk propagator through the equation of motion (2.21). Linking the previous elements together, we obtain

$$(C_{(23)}^{(2)} - m_{\mathrm{E}}^2)I(z_a, x_a; x_2, x_3) = (\nabla_a^2 - m_{\mathrm{E}}^2)I(z_a, x_a; x_2, x_3) \tag{B.17}$$

$$= K_{\Delta_\phi}(z_a, x_a; x_2)K_{\Delta_\phi}(z_a, x_a; x_3). \tag{B.18}$$

The quadratic Casimir acting on the points 3 and 4 commutes with the other coordinates, so we can write a differential equation relating the full exchange diagram to the contact term

$$(C_{(23)}^{(2)} - m_{\mathrm{E}}^2)J(x_1, x_2, x_2, x_3) = \int \frac{\mathrm{d}z_a\, \mathrm{d}x_a}{z_a^2}\Pi_{i=1}^4 K_{\Delta_\phi}(z_a, x_a; x_i) \tag{B.19}$$

$$= \frac{A}{(x_{13}x_{24})^{2\Delta_\phi}}\bar{D}_{\Delta_\phi\Delta_\phi\Delta_\phi\Delta_\phi}(z). \tag{B.20}$$

The same analysis holds for any two legs attached to a bulk-to-bulk propagator, though the final differential equation might depend on many variables.

---

[13] We write the transformations under the conformal group as vectors $\vec{L}_2 = (L_{-1}, L_0, L_1)$ acting on point 2.

B.2. Perturbative Polyakov blocks

Polyakov blocks and OPE expansion.

It will be useful to illustrate how Polyakov blocks and conformal blocks operate perturbatively. The four-point correlator of a scalar of conformal dimension Δ is

$$\langle \phi_\Delta(x_1)\phi_\Delta(x_1)\phi_\Delta(x_1)\phi_\Delta(x_1)\rangle = \frac{(C_\Delta)^4}{(x_{13}x_{24})^{2\Delta}} f(z) \tag{B.21}$$

$$f(z) = \sum_h c_{\Delta\Delta h}^2 z^{-2\Delta} G_h(z) = \sum_h c_{\Delta\Delta h}^2 z^{-2\Delta} P_h(z), \tag{B.22}$$

where G_h are the conformal blocks and $P_h(z)$ are the Polyakov blocks. The four-point conformal blocks in $d = 1$ are the eigenfunctions of the quadratic Casimir

$$G_h(z) = z^h {}_2F_1(h, h, 2h; z). \tag{B.23}$$

The Polyakov blocks are not eigenvalues of the quadratic Casimir and depend non-trivially on the exchanged and external dimension. Though the Polyakov blocks are not known in closed form in position sapce, their double-discontinuity is equal to that of the conformal blocks in the t-channel

$$\mathrm{dDisc}[z^{-2\Delta}P_h^{(t)}(z)] = \mathrm{dDisc}[z^{-2\Delta}G_h^{(t)}(z)]$$

$$= 2\sin^2\left(\frac{\pi}{2}(h - 2\Delta)\right)(1 - z)^{-2\Delta}G_h(1 - z). \tag{B.24}$$

The double-discontinuity of the Polyakov block in the t-channel is given by the replacement $z \to 1 - z$ since the Polyakov block is crossing-symmetric[14].

$$\mathrm{dDisc}[z^{-2\Delta}P_h^{(s)}(z)] = 2\sin^2\left(\frac{\pi}{2}(h - 2\Delta)\right)z^{-2\Delta}G_h(z). \tag{B.25}$$

If we expand the four-point correlator in a small strong coupling parameter ϵ

$$f(z) = f^0(z) + \epsilon f^1(z) + O(\epsilon^2), \tag{B.26}$$

one can look at the structure and properties of these two expansions. The first order is generalised free field theory where the spectrum is $\{0, h = 2\Delta + 2n\}$, and the correlator is obtained with the pairwise Wick contractions between fields

$$f^0(z) = 1 + z^{2\Delta} + \left(\frac{z}{1 - z}\right)^{2\Delta}. \tag{B.27}$$

The conformal decomposition

$$f^0(z) = 1 + \sum_n c_{2\Delta+2n,\Delta,\Delta}^2 G_{2\Delta+2n}(z), \tag{B.28}$$

---

[14] We choose a prefactor $\frac{1}{(x_{13}x_{24})^{2\Delta}}$ to have a crossing-symmetric function $f(z)$. However, we keep the normalisation of the blocks in equation (B.23) to be consistent with the literature and use the combination $z^{-2\Delta}P(z)$ to work with a truly crossing-symmetric quantity, without the need for a prefactor.

gives the OPE coefficients. Whereas the Polyakov blocks vanish at the position of the double trace operators

$$f^0(z) = P_{\Delta,0}(z) + \sum_n c_n^{(0)} P_{2\Delta+2n}(z), \tag{B.29}$$

giving the identity contribution in all channels.

$$P_{\Delta,0}(z) = 1 + z^{2\Delta} + \left(\frac{z}{1-z}\right)^{2\Delta}. \tag{B.30}$$

At first order in a perturbative expansion, assuming that there are no new exchanged operators[15], the spectrum is $h = \{0, 2\Delta + 2n + \epsilon\gamma_n^{(1)}\}$, where the identity operator receives no corrections. The first order OPE expansion is then

$$f^1(z) = \sum_n c_n^{(1)} G_n(z) + c_n^{(0)} \left(\frac{g\gamma_n}{2}\right)\partial_n G_n(z) \tag{B.31}$$

$$= \sum_n c_n^{(0)} \left(\frac{g\gamma_n}{2}\right)\partial_n P_n(z). \tag{B.32}$$

Only one term in the Polyakov block expansion is non vanishing in this case

$$f^1(z) = c_0^{(0)} \left(\frac{g\gamma_0}{2}\right)(\partial_n P_n)|_{n=0}(z). \tag{B.33}$$

If there is a new exchanged operator $\Delta_E \neq 2\Delta + 2n$ at this order ($c_{\Delta_E\Delta\Delta} = O(\sqrt{\epsilon})$), the expansion is changed by a factor:

$$f^1(z) = c_0^{(0)} \left(\frac{g\gamma_0}{2}\right)(\partial_n P_n)|_{n=0}(z) + c_{\Delta_E\Delta\Delta}^2 P_{\Delta_E}(z). \tag{B.34}$$

In the strong coupling language, this corresponds to having an exchange Witten diagram with exchange dimension Δ_E. Hence, the Polyakov blocks are given by exchange Witten diagrams, up to the contact diagram contribution from equation (B.33).

Polyakov blocks and exchange Witten diagrams.

The computation of the exchange Witten diagram in the main text (5.19) is the sum of solutions to second-order differential equations. The integration constants are provided by the three-point function and the symmetry of the correlator. The example given in the main text corresponding to the Polyakov block of external dimension $\Delta = 1$ and exchanged dimension $\Delta_E = 1$ can be computed with the toy model of a massless scalar theory in AdS$_2$ with a ϕ^3 interaction, this corresponds to the action

$$S_{\phi^3} = \int \frac{dt\,dz}{z^2} \left(\partial_\mu\phi\partial^\mu\phi - \frac{\lambda}{3!}\phi^3\right). \tag{B.35}$$

The leading order is given by GFF. The next to leading order ($O(\lambda)$) correlators come from the constant vertex giving the three point function

$$\langle\phi(x_1)\phi(x_2)\phi(x_3)\rangle = \frac{\lambda}{\pi^3} \frac{\pi^2}{2x_{12}x_{23}x_{13}}, \tag{B.36}$$

---

[15] At strong coupling, this means that the first order Witten diagrams are contact diagrams and not exchange diagrams.

and the OPE coefficient

$$c_{111} = \frac{\lambda}{2\pi}. \tag{B.37}$$

The first sub-leading term ($O(\lambda^2)$) in the four-point function is generated by the exchange diagram which contributes

$$\langle \phi(x_1)\phi(x_2)\phi(x_3)\phi(x_4) \rangle = \sum_{s,t,u} \lambda^2 J_{\Delta_E=1,\Delta=1}(x_1,\dots,x_4) \tag{B.38}$$

$$= \frac{\lambda^2}{\pi^5} \frac{\pi}{4} \frac{1}{(x_{13}x_{24})^2} P_{(1,1)}^{(0)}(z), \tag{B.39}$$

where $P_{(1,1)}^{(0)}(z)$ is written explicitly in equation (5.19) and has a small z expansion[16]

$$\langle \phi(x_1)\phi(x_2)\phi(x_3)\phi(x_4) \rangle = \frac{1}{(x_{13}x_{24})^2} \frac{\lambda^2}{4\pi^4} \left(\frac{c_1 - 6\zeta(3)}{z^2} + \frac{2(\pi^2 - 3c_2)}{3z} \right) + o\left(\frac{1}{z}\right). \tag{B.40}$$

The first term in the expansion is set to zero since it corresponds to a correction to the identity operator. The second term corresponds in the conformal s-channel OPE to

$$\frac{1}{(x_{13}x_{24})^2} \sum_h c_{11h}^2 z^{h-2} {}_2F_1(h,h,2h,z) = \frac{1}{(x_{13}x_{24})^2} \left(\frac{c_{111}^2}{z} + o\left(\frac{1}{z}\right) \right), \tag{B.41}$$

where by equating the expansions in the conformal and Polyakov blocks, this corresponds to $c_{\Delta_E \Delta \Delta}$ in equation (B.34). The known three-point function and the four-point OPE then give the solutions for the integration constants

$$c_1 = 6\zeta(3) \tag{B.42}$$

$$c_2 = -\frac{\pi^2}{6}, \tag{B.43}$$

and provide the correct numerical factor for the Polyakov block computed in the main text as well as the maximally symmetric and Regge-bounded function.

B.3. Higher weight exchange diagrams and bootstrap

The process done in the main text can be repeated for other exchanged weights, for example we have the s-channel exchanges

$$f_{\Delta_E=2}^{(s)}(z) = \frac{4c_2 - 4z\log^2(z) + 8z\,\log(z) + 2\,\log(1-z)(2z\,\log(z) - 4) + \frac{4\pi^2}{3}}{z^3}$$

$$\tag{B.44}$$

$$+ \frac{2(z-2)}{z^3}\left(c_1 - c_2\,\log(1-z) - \text{Li}_2(z)\log\left(\frac{1-z}{z^2}\right) \right.$$

$$\left. - \text{Li}_3(1-z) - 2\text{Li}_3(z) + \log\left(\frac{z}{1-z}\right)\log(1-z)\log(z) \right)$$

---

[16] We have kept the integration constants from (5.9).

$$f^{(s)}_{\Delta_E=3} = -\frac{2((z-6)z+6)(+3\mathrm{Li}_3(1-z)+\log(1-z)(\mathrm{Li}_2(z)+\log(1-z)\log(z)))}{z^4} \tag{B.45}$$

$$-\frac{6(z-2)(2\mathrm{Li}_2(z)+\log(1-z)\log(z))}{z^3}$$

$$+\frac{2\big(9z^2\log(z)+\big(\pi^2((z-6)z+6)-9\big(z^2+z-3\big)\big)\log(1-z)\big)}{3z^4}$$

$$+2\frac{\big(\pi^2(z-3)-9(z-4)\big)(z-1)}{z^4}$$

$$f^{(s)}_{\Delta_E=4} = -\frac{2(z-2)\big(z^2-10z+10\big)}{z^5}\left(\mathrm{Li}_2(z)\log\left(\frac{1-z}{z^2}\right)\right. \tag{B.46}$$

$$\left. +\,\mathrm{Li}_3(1-z)+2\mathrm{Li}_3(z)+\log(z)\log^2(1-z)-\log^2(z)\log(1-z)\right)$$

$$+\frac{2(11z^2-60z+60)(\log(1-z)-\log(z))\log(z)}{3z^4}$$

$$+\frac{8z(z(19z-90)+90)\log(z)-2(z-1)(z(76z-335)+310)\log(1-z)}{9z^5}$$

$$+\frac{10(z(2(104-9z)z-505)+330)+2\pi^2(z((336-25z)z-885)+610)}{9z^5}.$$

As we increase the weight of the exchanged operator, this seemingly increases the complexity of the solution, however, there are some patterns that are easy to spot. Notice that all transcendentality three terms have the same polynomial function multiplying them motivating the use a transcendentality ansatz [10]:

$$\sum_{n,i} r_{i,n}(z)T_{i_n}(z). \tag{B.47}$$

And inserting it in the differential equations, we obtain differential equations for the polynomials multiplying the transcendentality i functions for arbitrary weight Δ_E and arbitrary external weights Δ. In particular, the polynomials multiplying the transcendentality three terms remaining after the action of the Casimir differential operator will satisfy the homogeneous differential equation. Explicitly we have

$$r^{(s)}_{3,n} = c_n z^{-2\Delta-\Delta_E+1}\,{}_2F_1(1-\Delta_E, 1-\Delta_E; 2-2\Delta_E; z) \tag{B.48}$$

$$r^{(t)}_{3,n} = c_n(1-z)^{-2\Delta-\Delta_E+1}\,{}_2F_1(1-\Delta_E, 1-\Delta_E; 2-2\Delta_E; 1-z) \tag{B.49}$$

$$r^{(u)}_{3,n} = P_{\Delta_E-1}(2z-1). \tag{B.50}$$

The transcendentality two functions are multiplied by polynomials that satisfy inhomogeneous differential equations and are difficult to solve for general Δ_E. However, for specific cases, they are simple to solve. We can do this for example for higher exchanged weights and more

importantly, for higher-point correlators with exchanges. This analysis is beyond the scope of this paper and left for further investigation.

Appendix C. Multipoint Ward identity: a check

A concrete example of n-point correlators of fields at the boundary of AdS$_2$ is the dual setup of the defect CFT of operator insertions on the 1/2 BPS Wilson line in $\mathcal{N} = 4$ SYM studied at strong coupling in [1, 2]. In higher-point correlators, the first terms in the strong coupling expansion will originate from disconnected Witten diagrams. These first terms in the strong coupling expansion should satisfy the multipoint Ward identity presented in [36], therefore providing a perturbative check of these conjectured Ward identities

$$\sum_{k=1}^{n-3} \left(\frac{1}{2} \partial_{\chi_k} + \alpha_k \partial_{r_k} - (1 - \alpha_k) \partial_{s_k} \right) \mathcal{A}_{\Delta_1 \ldots \Delta_n} \Bigg|_{\substack{r_i \to \alpha_i \chi_i \\ s_i \to (1 - \alpha_i)(1 - \chi_i) \\ t_{ij} \to (\alpha_i - \alpha_j)(\chi_i - \chi_j)}} = 0, \tag{C.1}$$

where we use the notation of [36] in which the cross-ratios are defined as[17]

$$\chi_{i-1} = \frac{x_{1i} x_{n-1,n}}{x_{in} x_{1,n-1}} \tag{C.2}$$

$$r_{i-1} = \frac{(u_1 \cdot u_i)(u_{n-1} \cdot u_n)}{(u_i \cdot u_n)(u_1 \cdot u_{n-1})} \tag{C.3}$$

$$s_{i-1} = \frac{(u_1 \cdot u_n)(u_i \cdot u_{n-1})}{(u_i \cdot u_n)(u_1 \cdot u_{n-1})} \tag{C.4}$$

$$t_{i-1,j-1} = \frac{(u_i \cdot u_j)(u_1 \cdot u_n)(u_{n-1} \cdot u_n)}{(u_i \cdot u_n)(u_j \cdot u_n)(u_1 \cdot u_{n-1})}, \tag{C.5}$$

and the Ward identity is applied to the correlator of dimension $\Delta = 1$, SO(5) vectors expressed in terms of cross-ratios

$$\langle \Pi_{i=1}^6 u_{a_i} \Phi^{a_i}(x_i) \rangle = C(x_i, u_i) \mathcal{A}_{\Delta=1, n=6}(\chi_i, r_i, s_i, t_{i,j}), \tag{C.6}$$

where the prefactor

$$C(x_i, u_i) = \frac{(u_1.u_5)^2 (u_2.u_6)(u_3.u_6)(u_4.u_6)}{(u_1.u_6)(u_5.u_6)} \frac{x_{16}^2 x_{56}^2}{x_{15}^4 x_{26}^2 x_{36}^2 x_{46}^2}, \tag{C.7}$$

has been amputated. The strong coupling expansion of this quantity is given by the holographic dual studied in [1], where the dual of these particular fields are the fluctuations in the S^5 directions propagating in the AdS$_2$ minimal string surface. If we denote the strong coupling expansion parameter by g, we can expand the six-point function at strong coupling

$$\mathcal{A}_{\Delta=1, n=6}(\chi_i, r_i, s_i, t_{i,j}) = \mathcal{A}_{\Delta=1, n=6}^{(0)}(\chi_i, r_i, s_i, t_{i,j}) + g \mathcal{A}_{\Delta=1, n=6}^{(1)}(\chi_i, r_i, s_i, t_{i,j}) + O(g^2). \tag{C.8}$$

Given the Ward identity is coupling independent, each of the terms in this perturbative expansion should satisfy equation (C.1). The leading term, $\mathcal{A}_{\Delta=1, n=6}^{(0)}$, in the strong coupling

---

[17] The shift is the index of the cross-ratios is to have them ranging from 1 to $n - 3$.
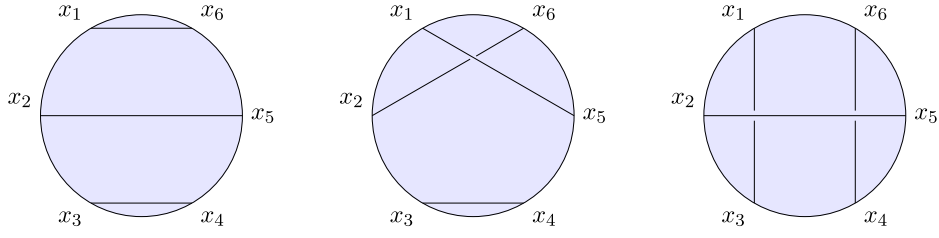
Figure 9. A non-exhaustive list of leading order disconnected Witten diagram. The overlapping lines are broken to indicate they are not vertices, it is not a non-planar contribution at strong coupling, since we are in the strict planar limit.

expansion corresponds to the simple Wick contractions where a few examples are drawn in figure 9.

Explicitly, performing these permutations, we find

$$
\mathcal{A}^{(0)}_{\Delta=1, n=6} = \frac{r_3 t_{1,2}}{(\chi_1 - \chi_2)^2 \chi_3^2} + \frac{r_2 t_{1,3}}{\chi_2^2 (\chi_1 - \chi_3)^2} + \frac{r_1 t_{2,3}}{\chi_1^2 (\chi_2 - \chi_3)^2}
$$
$$
+ \frac{s_1 t_{2,3}}{(\chi_1 - 1)^2 (\chi_2 - \chi_3)^2} + \frac{s_3 t_{1,2}}{(\chi_1 - \chi_2)^2 (\chi_3 - 1)^2}
$$
$$
+ \frac{s_2 t_{1,3}}{(\chi_2 - 1)^2 (\chi_1 - \chi_3)^2} + \frac{t_{1,2}}{(\chi_1 - \chi_2)^2} + \frac{t_{1,3}}{(\chi_1 - \chi_3)^2}
$$
$$
+ \frac{t_{2,3}}{(\chi_2 - \chi_3)^2} + \frac{r_2 s_1}{(\chi_1 - 1)^2 \chi_2^2} + \frac{r_3 s_1}{(\chi_1 - 1)^2 \chi_3^2}
$$
$$
+ \frac{r_1 s_2}{\chi_1^2 (\chi_2 - 1)^2} + \frac{r_1 s_3}{\chi_1^2 (\chi_3 - 1)^2} + \frac{r_2 s_3}{\chi_2^2 (\chi_3 - 1)^2} + \frac{r_3 s_2}{(\chi_2 - 1)^2 \chi_3^2}. \tag{C.9}
$$

For which, not only is the Ward identity satisfied, but each of the terms in equation (C.9) corresponding to the different R-symmetry channels individually satisfy this equation. As such, this is a trivial check of this Ward identity. The next-to-leading term corresponds to the disconnected diagram with one Wick contraction and a contact four-point function,

$$
\mathcal{A}^{(1)}_{\Delta=1, n=6}(\chi_i, r_i, s_i, t_{i,j}) = \frac{r_1 t_{2,3} G_4^{(1)}\left(\frac{\chi_1 (\chi_2 - \chi_3)}{\chi_2 (\chi_1 - \chi_3)} \right)}{\chi_1^2 (\chi_2 - \chi_3)^2} + \text{permutations}\,[(x_i, u_i)]. \tag{C.10}
$$

This corresponds to the permutations of which a few examples are given by the disconnected Witten diagrams in figure 10.

The four-point function is computed in [1] and can be written as

$$
\langle \Phi^{a_1}(x_1) \Phi^{a_2}(x_2) \Phi^{a_3}(x_3) \Phi^{a_4}(x_4) \rangle = \frac{\delta^{a_1}_{a_2} \delta^{a_3}_{a_4}}{(x_{12} x_{34})^2} G_4^{(1)}\left(\frac{x_{12} x_{34}}{x_{13} x_{24}} \right)
$$
$$
+ \text{permutations}\,[(x_i, u_i)] \tag{C.11}
$$

$$
G_4^{(1)}(\chi) = \frac{(\chi - 1)(\chi^2 + \chi + 2) \log((\chi - 1)^2)}{2\chi}
$$
$$
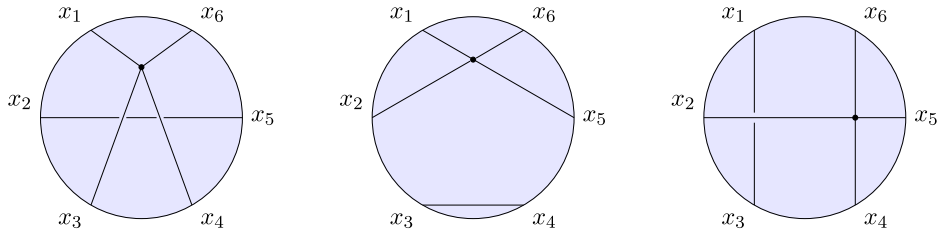- \frac{(\chi^2 - 2\chi + 2)(\chi^2 \log(\chi^2) - 2\chi + 2)}{2(\chi - 1)^2}. \tag{C.12}
$$

Figure 10. Some of the next-to-leading order disconnected Witten diagrams.

Just as in the GFF case, each of the *R*-symmetry channels also satisfy the Ward identities (C.1) individually. As a consequence, this is not constraining for the six-point function, but rather motivates the consistency of these Ward identities. This seems to follow from the fact that the disconnected contribution can be written as a product of correlators, each satisfying a Ward identity, though this is dependent on the crossing and analytic properties of the four-point function. While it does not give insight into the connected contribution, this seems to indicate a recursive method to prove this Ward identity for any disconnected correlators.

ORCID iDs

Gabriel Bliard ⓘ https://orcid.org/0000-0002-4824-3760

References

[1] Giombi S, Roiban R and Tseytlin A A 2017 Half-BPS Wilson loop and AdS_2/CFT_1 *Nucl. Phys.* B **922** 499

[2] Liendo P, Meneghelli C and Mitev V 2018 Bootstrapping the half-BPS line defect *J. High Energy Phys.* JHEP10(2018)077

[3] Beccaria M, Giombi S and Tseytlin A A 2019 Correlators on non-supersymmetric Wilson line in $N = 4$ SYM and AdS_2/CFT_1 *J. High Energy Phys.* JHEP05(2019)122

[4] Bianchi L, Bliard G, Forini V, Griguolo L and Seminara D 2020 Analytic bootstrap and Witten diagrams for the ABJM Wilson line as defect CFT_1 *J. High Energy Phys.* JHEP08(2020)143

[5] Barrat J, Liendo P and Plefka J 2021 Two-point correlator of chiral primary operators with a Wilson line defect in $N = 4$ SYM *J. High Energy Phys.* JHEP05(2021)195

[6] Ferrero P and Meneghelli C 2021 Bootstrapping the half-BPS line defect CFT in $N = 4$ supersymmetric Yang–Mills theory at strong coupling *Phys. Rev.* D **104** L081703

[7] Paulos M F, Penedones J, Toledo J, van Rees B C and Vieira P 2017 The *S*-matrix bootstrap: I. QFT in AdS *J. High Energy Phys.* JHEP11(2017)133

[8] Ouyang H 2019 Holographic four-point functions in Toda field theories in AdS_2 *J. High Energy Phys.* JHEP04(2019)159

[9] Mazáč D 2017 Analytic bounds and emergence of AdS_2 physics from the conformal bootstrap *J. High Energy Phys.* JHEP04(2017)146

[10] Ferrero P, Ghosh K, Sinha A and Zahed A 2020 Crossing symmetry, transcendentality and the Regge behaviour of 1D CFTs *J. High Energy Phys.* JHEP07(2020)170

[11] Beccaria M, Jiang H and Tseytlin A A 2020 Boundary correlators in WZW model on AdS_2 *J. High Energy Phys.* JHEP05(2020)099

[12] Beccaria M, Jiang H and Tseytlin A A 2019 Supersymmetric Liouville theory in AdS_2 and AdS/CFT *J. High Energy Phys.* JHEP11(2019)051

[13] Beccaria M and Tseytlin A A 2019 On boundary correlators in Liouville theory on AdS_2 *J. High Energy Phys.* JHEP07(2019)008

[14] Beccaria M, Jiang H and Tseytlin A A 2019 Non-Abelian Toda theory on AdS$_2$ and duality *J. High Energy Phys.* JHEP09(2019)036

[15] Di Pietro L and Stamou E 2018 Operator mixing in the ϵ-expansion: scheme and evanescent-operator independence *Phys. Rev.* D **97** 065007

[16] Maldacena J, Michelson J and Strominger A 1999 Anti-de Sitter fragmentation *J. High Energy Phys.* JHEP02(1999)011

[17] Gross D J and Rosenhaus V 2017 A line of CFTs: from generalized free fields to SYK *J. High Energy Phys.* JHEP07(2017)086

[18] Maldacena J and Stanford D 2016 Remarks on the Sachdev–Ye–Kitaev model *Phys. Rev.* D **94** 106002

[19] Witten E 1998 Anti de Sitter space and holography *Adv. Theor. Math. Phys.* **2** 253

[20] D'Hoker E, Freedman D Z, Mathur S D, Matusis A and Rastelli L 1999 Graviton and gauge boson propagators in AdS(d + 1) *Nucl. Phys.* B **562** 330

[21] D'Hoker E, Freedman D Z, Mathur S D, Matusis A and Rastelli L 1999 Graviton exchange and complete four point functions in the AdS/CFT correspondence *Nucl. Phys.* B **562** 353

[22] D'Hoker E, Freedman D Z and Rastelli L 1999 AdS/CFT four point functions: how to succeed at z integrals without really trying *Nucl. Phys.* B **562** 395

[23] Freedman D Z, Mathur S D, Matusis A and Rastelli L 1999 Comments on four-point functions in the CFT/AdS correspondence *Phys. Lett.* B **452** 61

[24] Rastelli L and Zhou X 2017 Mellin amplitudes for AdS$_5$ × S^5 *Phys. Rev. Lett.* **118** 091602

[25] Zhou X 2019 Recursion relations in Witten diagrams and conformal partial waves *J. High Energy Phys.* JHEP05(2019)006

[26] Zhou X 2020 How to succeed at Witten diagram recursions without really trying *J. High Energy Phys.* JHEP08(2020)077

[27] Dolan F A and Osborn H 2001 Conformal four point functions and the operator product expansion *Nucl. Phys.* B **599** 459

[28] Penedones J 2011 Writing CFT correlation functions as AdS scattering amplitudes *J. High Energy Phys.* JHEP03(2011)025

[29] Fitzpatrick A L, Kaplan J, Penedones J, Raju S and van Rees B C 2011 A natural language for AdS/CFT correlators *J. High Energy Phys.* JHEP11(2011)095

[30] Paulos M F 2011 Towards Feynman rules for Mellin amplitudes in AdS/CFT *J. High Energy Phys.* JHEP10(2011)074

[31] Bissi A, Sinha A and Zhou X 2022 Selected topics in analytic conformal bootstrap: a guided journey (arXiv:2202.08475)

[32] Gopakumar R, Kaviraj A, Sen K and Sinha A 2017 A Mellin space approach to the conformal bootstrap *J. High Energy Phys.* JHEP05(2017)027

[33] Rastelli L and Zhou X 2018 How to succeed at holographic correlators without really trying *J. High Energy Phys.* JHEP04(2018)014

[34] Mezei M, Pufu S S and Wang Y 2017 A 2D/1D holographic duality (arXiv:1703.08749)

[35] Bianchi L, Bliard G, Forini V and Peveri G 2021 Mellin amplitudes for 1D CFT *J. High Energy Phys.* JHEP10(2021)095

[36] Barrat J, Liendo P, Peveri G and Plefka J 2021 Multipoint correlators on the supersymmetric Wilson line defect CFT (arXiv:2112.10780)

[37] Alday L F, Henriksson J and van Loon M 2018 Taming the ϵ-expansion with large spin perturbation theory *J. High Energy Phys.* JHEP07(2018)131

[38] Lemos M, Liendo P, Meneghelli C and Mitev V 2017 Bootstrapping $N = 3$ superconformal theories *J. High Energy Phys.* JHEP04(2017)032

[39] Mazáč D 2019 A crossing-symmetric OPE inversion formula *J. High Energy Phys.* JHEP06(2019)082

[40] Gopakumar R, Kaviraj A, Sen K and Sinha A 2017 Conformal bootstrap in Mellin space *Phys. Rev. Lett.* **118** 081601

[41] Polyakov A M 1974 Non-Hamiltonian approach to conformal quantum field theory *J. Exp. Theor. Phys.* **39** 10 https://ui.adsabs.harvard.edu/abs/1974JETP

[42] Mazac D and Paulos M F 2019 The analytic functional bootstrap: II. Natural bases for the crossing equation *J. High Energy Phys.* JHEP02(2019)163

[43] Freedman D Z, Mathur S D, Matusis A and Rastelli L 1999 Correlation functions in the CFT$_d$/AdS$_{d+1}$ correspondence *Nucl. Phys.* B **546** 96

[44] Mack G 2009 *D*-Independent representation of conformal field theories in *D* dimensions via transformation to auxiliary dual resonance models. Scalar amplitudes (arXiv:0907.2407)

[45] Penedones J 2016 TASI lectures on AdS/CFT (arXiv:1608.04948)

[46] Wilcox R M 1967 Exponential operators and parameter differentiation in quantum physics *J. Math. Phys.* **8** 962

[47] Blanes S, Casas F, Oteo J A and Ros J 2009 *Phys. Rep.* **470** 151

[48] Costa M S, Gonçalves V and Penedones J 2014 Spinning AdS propagators *J. High Energy Phys.* JHEP09(2014)064